CHEMMEDCHEM

CHEMISTRY ENABLING DRUG DISCOVERY

Accepted Article

Title: Structure-activity relationships of 1-Benzoylazulenes at the OX1 and OX2 orexin receptors

Authors: Turku Ainoleena, Teppo O Leino, Lasse Karhu, Jari Yli-Kauhaluoma, Jyrki P Kukkonen, Erik A. A Wallén, and Henri Xhaard

To be cited as: *ChemMedChem* 10.1002/cmdc.201900074

Link to VoR: http://dx.doi.org/10.1002/cmdc.201900074

A Journal of

ChemPubSoc Europe

WILEY-VCH

www.chemmedchem.org

WILEY-VCH

FULL PAPER

Structure-activity relationships of 1-benzoylazulenes at the OX_1 and OX_2 orexin receptors

Ainoleena Turku[+],[a],[b] Teppo O. Leino[+],[a] Lasse Karhu,[a] Jari Yli-Kauhaluoma,[a] Jyrki P. Kukkonen[b],[c] Erik A. A. Wallén,[a] and Henri Xhaard*[a]

[a] Dr. A. Turku, 0000-0003-0959-7221, Dr. T. O. Leino, 0000-0003-2582-7971, Dr. L. Karhu, 0000-0001-6432-8580, Prof. J. Yli-Kauhaluoma, 0000-0003-0370-7653, Dr. E. A. A. Wallén, 0000-0002-2269-5179, Dr. H. Xhaard 0000-0002-3000-7858
Drug Research Program, Division of Pharmaceutical Chemistry and Technology, Faculty of Pharmacy
University of Helsinki
P.O. Box 56, FI-00014 University of Helsinki, Finland
E-mail: henri.xhaard@helsinki.fi

[b] Dr. A. Turku, Prof. J. P. Kukkonen, 0000-0002-6989-1564
Department of Veterinary Biosciences, Faculty of Veterinary Medicine
University of Helsinki
P.O. Box 66, FI-00014 University of Helsinki, Finland

[c] Prof. J. P. Kukkonen
Department of Physiology, Faculty of Medicine
University of Helsinki
P.O. Box 63, FI-00014 University of Helsinki, Finland

[+] These authors contributed equally to this work.

Supporting information for this article is given via a link at the end of the document.

Abstract: We demonstrated previously the potential of di- or tri-substituted azulenes as ligands (potentiators, weak agonists and antagonists) of the orexin receptors. Here, we investigated 27 1-benzoylazulene derivatives, uncovering seven potentiators of the orexin response on OX_1 and two weak dual orexin receptor agonists. For potentiators, replacement of the azulene scaffold by indole retained the activity of four out of six compounds. The structure-activity relationships for agonism and potentiation can be summarized into a bicyclic aromatic ring system substituted with two hydrogen-bond acceptors (1-position, benzoyl; 6-position, carboxyl/ester) within 7–8 Å of each other; a third acceptor at the 3-position is also well tolerated. The same pharmacophoric signature is found in the preferred conformations of the orexin receptor agonist Nag26 from molecular dynamics simulations. Subtle changes switch the activity between weak agonism and potentiation, suggesting overlapping binding sites.

Introduction

The orexin (hypocretin) system, orexin receptors OX_1 and OX_2 and peptide ligands orexin-A and orexin-B, regulates sleep/wake cycle.[1–3] It has also been associated with nociception, addiction and stress response.[4–6] Unlike orexin receptor antagonists, which have been actively pursued by the pharmaceutical industry for the treatment of insomnia, small molecular agonists or compounds that potentiate the effects of the endogenous orexin peptides have received less attention.[3,7–9] Agonists could be useful, for example, in the treatment of narcolepsy or certain types of cancer.[10,11] Potentiators would have applications in orexin receptor activation therapies in conditions where the production of endogenous peptides is not fully terminated.

Previously, we have successfully explored azulene-based compounds for targeting orexin receptors.[12] Following an *in-silico*-guided selection, we synthesized 33 compounds, among which we identified promising azulenes acting as orexin receptor antagonists with binding affinities at low micromolar level, as weak orexin receptor agonists (compounds **1** and **2**, Figure 1), and/or as potentiators of the orexin-A response on the OX_1 (but not the OX_2) receptors. Azulene is an aromatic bicycle composed of fused five-membered and seven-membered hydrocarbon rings, and it resembles other ring systems found in drug molecules. It caught our interest because of its characteristic dipole moment[13] and its amenability to substitutions at multiple positions, which makes it well suited to occupy the site of the amphipatic C-terminus of the endogenous orexin peptide.[14] Furthermore, the azulene scaffold has scarcely been used in medicinal chemistry: only a few examples of azulenes are found in the scientific literature, which is reflected in that, at times of this study, no 1-benzoylazulenes could be identified in the ChEMBL database. The published compounds have pre-clinical applications as antiulcer, antidiabetic, anticancer and pro-erectile agents.[15–18] Notably, the azulene framework has been previously used to target the orthosteric site in G protein-coupled dopamine D_4 receptors.[13]

In this study, we expanded the chemical space around the azulene-scaffolded compounds that we previously reported, with the objective to challenge the two aspects of the azulene ring that had initially attracted us: the scaffold itself and the presence of a dipole moment. In the original set of 33 compounds the active ones bore a benzoyl group at the 1-position and carboxyl or ester groups at the 6-position, while a few compounds with only one of these features were inactive (as an example compound **3** in Figure 2). We thus synthesized and tested 21 new 1,6-disubstituted azulenes. At the 1-position, we aimed to modify the benzoyl group either by polar substitutions or by replacing it with other aromatic groups, amide derivatives or oxoamide derivatives. The carboxyl and ester groups at the 6-position were replaced by amide derivatives. In these compounds, the groups at the 6-position were linked directly to the azulene scaffold (as in **1**), since synthetic modifications of the ester linked with a methylene group (as in **2**) were expected to be problematic (see reference[12]). The

importance of the azulene scaffold was furthermore tested by indole replacements (set of six indole-scaffolded compounds).

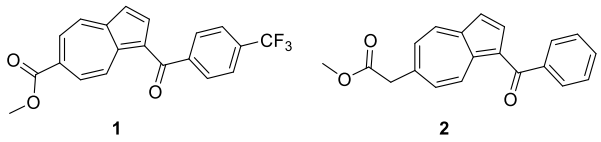

1 2

Figure 1. The weak orexin receptor agonists **1** and **2** presented in [12].

Results and Discussion

Chemistry

The synthesis of the starting materials **4** and **20** has been described previously.[12] Ketone derivatives of **4** were obtained applying the modified Vilsmeier–Haack reaction conditions (Scheme 1). As the reactions gave only low to moderate yields, the unreacted starting material was recovered and used in the synthesis of other ketone derivatives. However, the starting material obtained this way contained traces of methyl 1-chloroazulene-6-carboxylate, which had formed as a side product in the applied reaction conditions. Consequently, in the case of **9** the side product **10** was also obtained. Of note, our attempts to synthesize **11** with this method failed and no product was observed.

2-Oxoacetamide and amide derivatives of **4** were synthesized by treating **4** first with oxalyl chloride or phosgene, followed by the addition of an appropriate base. The method has previously been described for 2-oxoacetamide derivatives.[19] However, phosgene did not prove to be as reactive as oxalyl chloride with the 1-position of azulene, thus we could not use the same reaction conditions. Indole derivatives with benzoyl group at the 3-position were obtained in low yields (2–3%) with the trisubstituted indoles **35** and **36** being the major products.

Activity assessment of the azulene-based derivatives

We first screened the Ca^{2+} responses of the 21 azulene derivatives using a Ca^{2+} elevation assay in Chinese hamster ovary-K1 (CHO) cells heterologously expressing high densities of human OX_1 and OX_2 receptors (Figure 2).[20,21] Ca^{2+} elevation is a prominent response to orexin receptor activation, and would thus reveal orexin receptor agonism,[22] yet it may also be caused by other proteins. To test if the observed responses were orexin receptor-mediated, we additionally screened these 21 compounds in presence of orexin receptor antagonists with nanomolar binding affinities (SB-334867 for OX_1 and TCS-1102 for OX_2[23,24]), as described in reference[25].

Three compounds, **15**, **26**, and **28**, showed Ca^{2+} responses of 5–12% in OX_1 and 8–18% OX_2-expressing cells (Figure 2 A; for full data see Supporting Information Table 1). In the presence of the orexin receptor antagonists, the responses of **26** and **28** were partially blocked, while the responses to **15** were unaffected indicating that the responses to **15** were not orexin receptor-mediated. Thus, we continued the studies with **26** and **28**, but not **15**.

Then, we scrutinized the Ca^{2+} responses of **1** (the parent compound), **26** and **28** with concentration-response measurements in OX_1 and OX_2 receptor-expressing cells, as well as in control CHO cells (not expressing orexin receptors). Additionally, we studied further the previously reported compound **37** (compound **19** in reference[12]). In previous work, **37** demonstrated binding to orexin receptors (with functional K_i values of 7.5 µM and 4.9 µM on the OX_1 and OX_2 receptors, respectively[12]), but no Ca^{2+} response in the agonist activity screening we conducted at 10 µM concentration. Here we show that **37** acts as a weak orexin receptor agonist at higher concentrations.

As a result, none of the scrutinized compounds were especially potent. The highest responses were seen for compound **37** at 45 µM concentration, with responses of 18.3 ± 3.0% and 17.5 ± 6.4% of the E_{max} of orexin-A, respectively, on OX_1 and OX_2 receptors (Figure 2F). Compounds **1**, **28** and **37** showed concentration-dependent Ca^{2+} responses, both total and orexin receptor-specific (Figure 2C, 2E and 2F). In contrast, the responses to compound **26** dropped at the 32 µM concentration (Figure 2D), which may be due to solubility issues at this high concentration level. At 32 µM concentration, **37** did not form colloidal aggregates,[12] cause a fluorescence of its own at the utilized wavelengths, or show morphological changes indicating fast cell death (as examined by a visual inspection after running the assay similarly to reference[26]; data not shown). Furthermore, the use of control CHO cells should allow detection of non-orexin receptor-mediated effects leading to Ca^{2+} elevation. Altogether, these demonstrate that compounds **1**, **26**, **28** and **37** indeed act as weak orexin receptor agonists.

In addition to the agonist activities, we screened these 21 compounds for functional potentiation effects on the response to orexin-A. It should be noted that the assay cannot discriminate between weak agonists and ago-PAMs (compounds that have both agonist and positive allosteric modulator activities), as the increase of the intracellular Ca^{2+} levels, which is a hallmark of the orexin receptor activation, potentiates directly the downstream signaling machinery and thus gives a positive signal.[12,21,27–30] Compounds **5**, **6** and **27** potentiated the response to orexin-A on OX_1 receptors by 1.4-, 1.6- and 1.3-fold, respectively, at 10 µM concentration (Supporting information Figure 1 and Supporting information Table 1). Additionally, compounds **10** (OX_1), **16** (both receptor subtypes), **19** (OX_2) and **24** (OX_1) showed a weak potentiating effect, but comparison with their effect on the control ATP response suggested that these are not mediated specifically by orexin receptors (Supporting information Table 1). We additionally tested the ability of 13 previously reported compounds (**10**, **12**–**13**, **15**–**16**, **18**, **20**–**25**, and **30** in reference[12]) to potentiate the orexin-A response; none of these were found to potentiate the effects of orexin-A (data not shown).

Systematic exploration of the azulene derivatives

This manuscript develops a pharmacophore hypothesis where two hydrogen bond acceptors distant from 7–8 Å are important for the activity (potentiation, agonism) of 1-benzoylazulene-based compounds. Altogether, 54 azulene-based compounds (four of them as mixtures) have been screened in the Ca^{2+} elevation assay for their agonist and potentiation activities combining this and previous work.[12] As discussed below, the hypothesis does fit the molecular structures of the five weak agonists and 11 potentiators identified so far. Some compounds that possess this pharmacophoric signature are inactive, which can be explained

by other unfitting substituents. We wrap-up the hypothesis in the conclusion of this manuscript.

This section focuses on the analysis of structure-activity relationships. We follow the ability of the compounds to potentiate orexin response or to induce signaling through Ca^{2+} elevation, which are complex and interconnected phenomena (see above). Here, binding to the orexin receptors is not evaluated, in contrast to reference[12], where we measured displacement of [^{125}I]-orexin-A. This is because in previous work the binding data appeared difficult to interpret due to the ability of some compounds to potentiate the [^{125}I]-orexin-A binding.[12]

The expanded data support the postulate that the carboxyl or ester groups at the 6-position are useful for weak agonism and/or potentiation: 88% (14/16) of the active compounds have these functional groups, while overall acid or ester are found in 67% (36/54) of the tested compounds (Table 1; for more detailed SAR data see the Supporting information Table 2). Di-substituted compounds (with a hydrogen atom at the 3-position) appear active approximately as often as tri-substituted compounds: 39% (11/28) and 36% (5/14) of all such compounds, respectively (Supporting information Table 2). At the 6-position, a set of seven amide derivatives was explored leading to the identification of the agonist hits **26** and **28**, which bear an additional hydrogen bonding group at the 6-position when compared to the original carboxylic acids and esters (pyridine in **26**, and hydroxyl in **28**; Table 1; Supporting information Table 2).

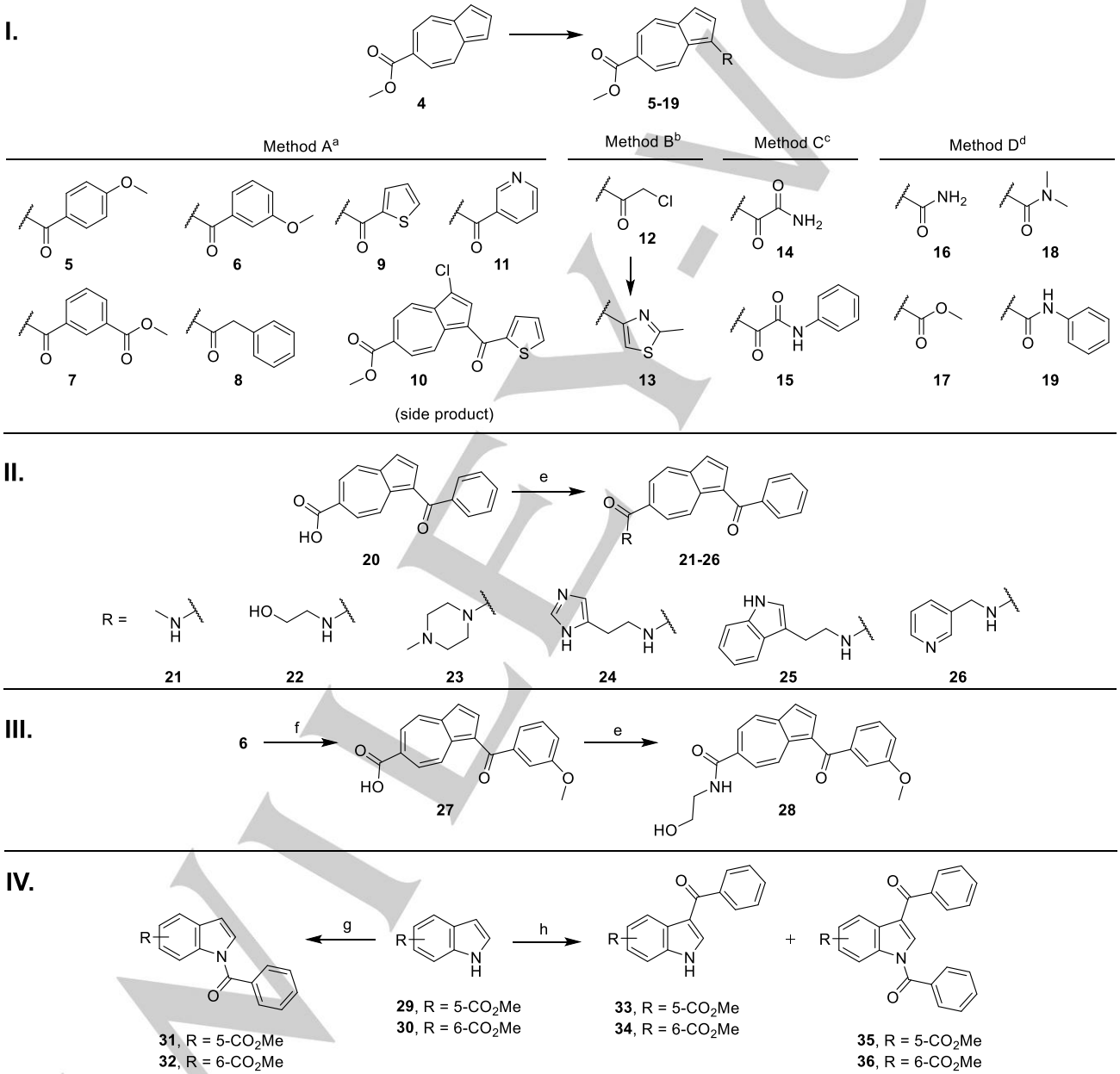

Scheme 1. Synthesis of compounds 5–36. Reagents and conditions: (a) An appropriate *N,N*-dimethylbenzamide, $POCl_3$, 1,4-dioxane, mw, 100 °C, 4–5 h, 22% (**5**), 18% (**6**), 44% (**7**), 31% (**8**), 29% (**9**), 0% (**11**); (b) i) 2-Chloro-*N,N*-diethylacetamide, $POCl_3$, 1,4-dioxane, mw, 100 °C, 2 h, 33%, ii) Thioacetamide, EtOH, mw, 120 °C, 30 min, 71%; (c) i) Oxalyl chloride, toluene, rt, 1 h, ii) An appropriate amine, DCM, 10–30 min, 64% (**14**), 50% (**15**); (d) i) Phosgene, toluene, 80 °C, overnight, ii) An appropriate amine, 0 °C, 15–30 min, 35% (**16**), 9% (**17**), 49% (**18**), 84% (**19**); (e) i) EDC·HCl, HOBt·H_2O, DMF, 0 °C, 15 min, rt, 1 h, ii) An appropriate amine derivative, rt, 1–2.5 h, 79% (**21**), 85% (**22**), 88% (**23**), 49% (**24**), 81% (**25**), 80% (**26**), 87% (**28**); (f) NaOH, THF, MeOH, H_2O, rt, 30 min, 98%; (g) Benzoyl chloride, Et_3N, DCM, rt, 23 h, 59% (**31**), 22% (**32**); (h) *N,N*-Dimethylbenzamide, $POCl_3$, mw, 100 °C, 1–3 h, 2% (**33**), 3% (**34**), 23% (**35**), 48% (**36**).

10.1002/cmdc.201900074

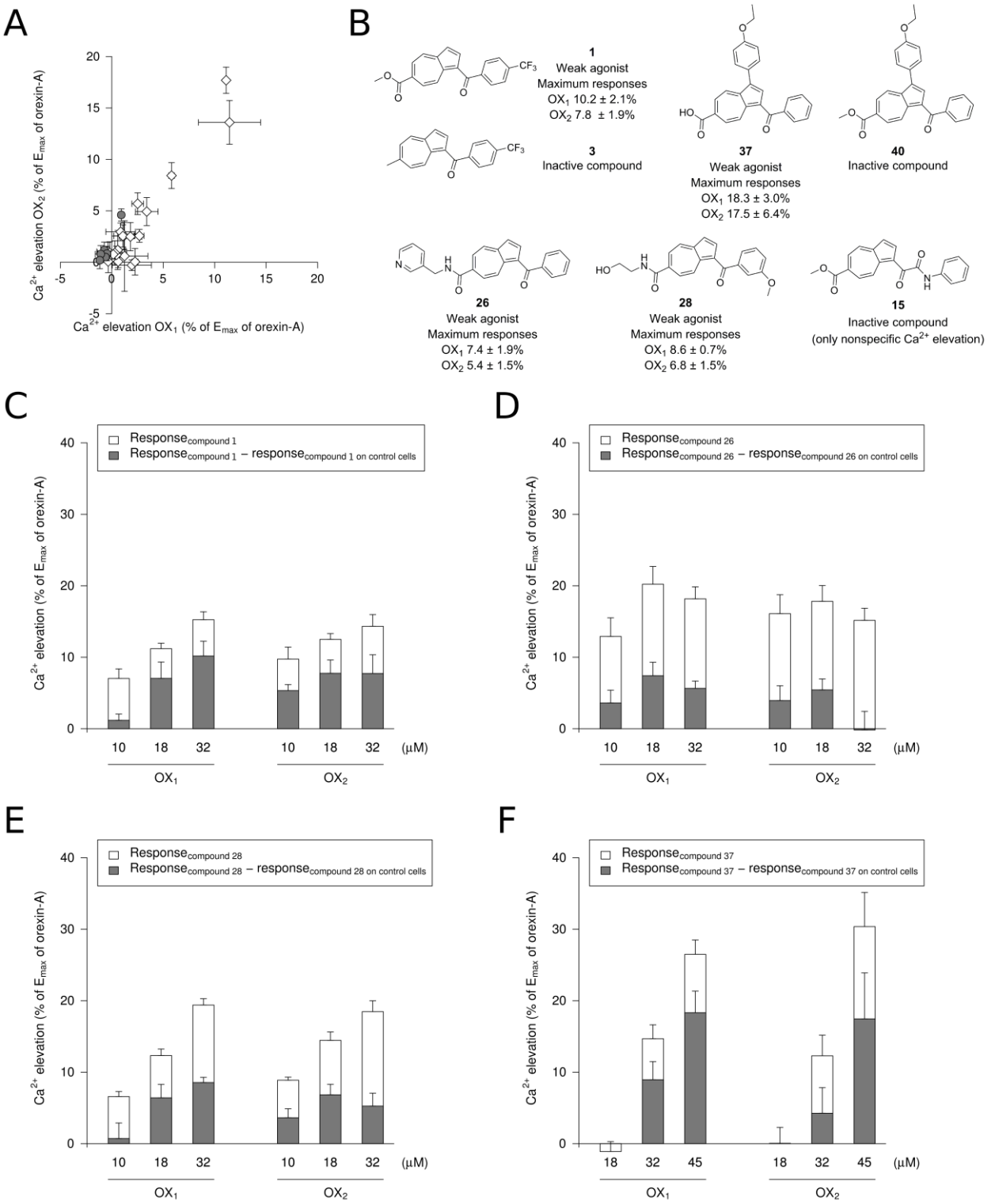

Figure 2. A. Screening of Ca^{2+} responses of all 21 azulene-based and 6 indole-based compounds at 10 μM concentration. Azulene derivatives are presented as hollow diamonds and indole derivatives as filled circles. **B.** Structures of compounds **15**, **26** and **28** that displayed the highest Ca^{2+} responses in the screening, and previously disclosed compounds **1**, **3**, **37** and **40**.[12] **C–F.** Total and orexin receptor-specific Ca^{2+} responses of **1** (C; 10 μM data from reference[12]), **26** (D), **28** (E), and **37** (**F**). Ca^{2+} responses are given as a percentage of the maximal response (E_{max}) of orexin-A. The responses were separately normalized to the E_{max} of orexin-A for each independent experiment before averaging. n=3–6.

Interestingly, the compounds with smaller amide substituents, primary carboxamide and methylcarboxamide (compound **21**), were inactive. The functional role as agonist or potentiator appears mediated by subtle changes. All five agonist hits, **1**, **2**, **26**, **28** and **37**, have either unsubstituted or substituted benzoyl group at the 1-position (Table 1). The agonist hit **1** can be shifted to a

potentiator by replacing the 4-trifluoromethylbenzoyl at the 1-position with either 3-methoxybenzoyl (compound **6**), or 4-methoxybenzoyl (compound **5**; Table 1). The unsubstituted benzoyl group in this position leads also to a potentiation effect (compound **38**), which however may be due to nonspecific Ca^{2+} elevation.[12] Nonetheless, when adding an iodine atom or a benzoyl group to the 3-position of **38**, the potentiation effect can be robustly ascribed to be mediated through the orexin receptors (Table 1). The other ten alterations of the 1-position of compound **1** (both those lacking the aryl ring and those having it combined with longer substituents or linkers) were not tolerated neither in terms of agonism nor potentiation (Supporting information Table 2). This emphasizes the importance of the 1-benzoylazulene-scaffold for the active compounds.

Table 1. Main structure-activity relationships (SARs) for compounds reported in this study (named compounds) and in reference[12] (compound names not shown). All potentiator hits acted only on the OX_1 receptor, whereas weak agonists had activity on both receptor subtypes.

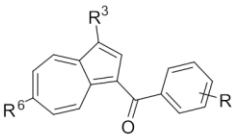

	R →	H	4-CF_3	3-methoxy	4-methoxy	H	H	H
R^6↓	R^3→	H	H	H	H	I	benzoyl	4-ethoxy-phenyl
				**27**				**37**
								
		**21**						
								
		**38**[a]	**1**	**6**	**5**		**39**	**40**
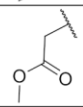		**2**						
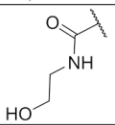		**22**[a]		**28**				
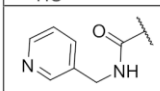		**26**						
Agonist hit		2	1	1				1
Potentiator		1	3	2	1	1	3	
Inactive		4						1

[a]non-orexin receptor-mediated Ca^{2+} response caused by the compound

Taken together, these data support that two hydrogen bond acceptors at 7–8 Å distance are important for the activity (potentiation, agonism) of 1-benzoylazulene-based compounds. All active compounds have a benzoyl group at the 1-position; for the di-substituted compounds (hydrogen atom at the 3-position), a small hydrogen bonding functionality at the 3- or 4-positions of this group seems also beneficial (compare e.g. compound **6** with compound **38**). Furthermore, for the di-substituted compounds ester and amide groups are observed at the 6-position of the agonist hits and a carboxyl group only at the 6-position of the potentiator hits. The observation that azulene derivatives can be shifted to compounds with different types of activity by minor changes suggest that they act at overlapping binding sites. In this case, potentiation may act through orexin receptor dimers/oligomers.[12] We are currently experimentally testing this hypothesis.

Importance of the core structure and the arrangement of substituents

Given the central role played by the 1-benzoylazulene-scaffold towards biological activities, we investigated its replacement by 1-benzoyl- or 3-benzoyl-indoles. As a ring structure, indole resembles azulene, but represents a fusion of a six- and a five-membered ring (not seven and five as in an azulene). Azulene is a large and rigid ring structure, and the designed compounds present a relatively narrow conformational space (usually six or less rotatable bonds). When designing the indole-based compounds, we decided to rely on the potentiation abilities that are more robust than the relatively weak agonist activities; we thus synthesized indole analogs for **38** and **39**, potentiators of Ca^{2+} response to orexin-A.[12] The indole scaffold does not offer spatially the exact substitution point corresponding to the 6-position of the azulene core, and thus altogether six benzoyl-indole derivatives were needed to mimic these two benzoyl-azulenes (Figure 3). The synthesis of the indole-scaffolded compounds is presented in the Scheme 1-IV.

Among the analogs of **38**, only **31** and **34** with substituents at exactly same spatial locations as those of the parent compound potentiated the response to orexin-A (respectively 1.9- and 1.4-fold at 10 µM concentration on OX_1 receptors; Figure 3A). Furthermore, **31** triggered non-orexin receptor-mediated Ca^{2+} elevation on OX_2 (but not OX_1; Figure 2A, filled circles; Supporting Information Table 1). At 10 µM, both analogs of **39** potentiated the orexin-A response 1.7-fold (Figure 3A and 3C). Additionally, **31**, **35** and **36** did not affect the response to sub-EC_{50} ATP indicating that the observed potentiation effect is orexin receptor-mediated (Figure 3B).

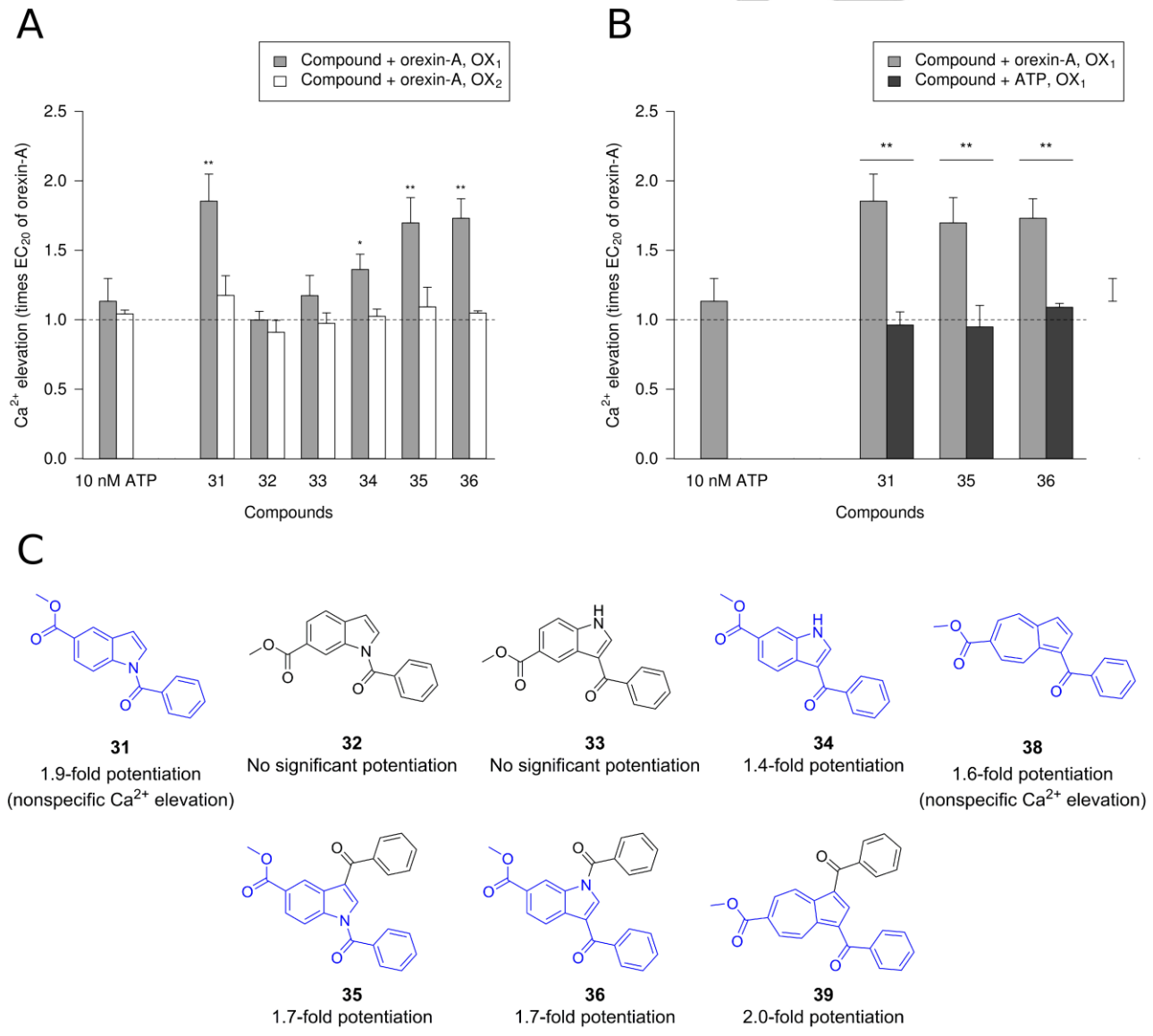

Figure 3. A. The effects of the indole derivatives at 10 µM concentration on the orexin-A response in the Ca^{2+} elevation assay. **B.** The three indole derivatives with the highest effect on orexin-A response in OX_1 receptors elicited by 0.03–0.04 nM orexin-A and 60 nM ATP (corresponding to the EC_{20} of each ligand). The responses were separately normalized to the control orexin-A or ATP response, respectively, for each independent experiment before averaging. The significances were calculated for the Ca^{2+} responses as compared with the corresponding control; non-marked significance indicates that the response of the compounds were

not significantly higher than the corresponding control. *P < 0.05, **P < 0.01; n = 3−4. **C.** The structures of the indole derivatives and the corresponding azulene-based compounds **38** and **39** reported in reference[12]. The structural framework present in all active compounds is highlighted in blue.

Changing the azulene scaffold to indole for **38** (as in **31** and **34**) and **39** (as in **35** and **36**) led only to a minor change in activities (Figure 3C). This shows that other aromatic core structures can be tolerated as a scaffolding unit to make orexin receptor potentiators; this would deserve more attention by studying other aromatic and non-aromatic scaffold hops in the future. Additionally, the location of the indole nitrogen had only a minor role on the activity, even though the non-substituted nitrogen atom of **34** seemed beneficial in terms of the non-orexin receptor-dependent Ca^{2+} elevation (when compared to both **31** and **38**). The inactive indole-based compounds **32**–**33** have clear difference in overall shape when compared to the active indole- and azulene-based compounds (Figure 3C); the carbonyl functionalities of **32** and **33** are approximately 1.5 Å closer to each other than those of the active compounds. This observation is consistent with the hypothesis presented in the beginning of this study that two hydrogen bond acceptors separated by 7–8 Å are important for the activity of azulene-based and related compounds.

Electrostatic considerations

We then set up to study the electronic distributions and the molecular (net) dipole moments for a small set of representative compounds using quantum mechanics (QM) calculations. Because of the computational costs, we restricted ourselves to four closely related compounds: **35** (indole-based potentiator), **37** (azulene-based agonist), **39** (azulene-based potentiator) and **40** (inactive azulene). We complemented the analysis by studying the agonist hits **1**, **2**, **26** and **28**, the docked agonist Nag26 (**41**), and the co-crystallized antagonists EMPA (**42**; PDB ID 5WQC[31]) and suvorexant (**43**; PDB ID 4S0V[32]).

Electronegative regions

For the active compounds, the calculations predictably highlight that the hydrogen-bond accepting regions are electron-rich. For example in the structure of the agonist hit **37**, these regions are strongly electronegative – a carboxyl functionality at the 6-position and carbonyl oxygen of the benzoyl group at the 1-position – and within a 7.4 Å distance from each other (Figure 4A; Table 2). When studying the weak agonist hits **1**, **2**, **26** and **28**, the presence of two electronegative regions separated by approximately 7 Å was also seen (Supporting information Figure 2). Unlike these di-substituted compounds though, **37** has a third electronegative region corresponding to the 4-ethoxyphenyl oxygen at the 3-position. Interestingly, in compound **40**, the inactive ester analog of **37**, these three electron-rich regions are present as well but they are notably weaker than those of **37** (Figure 4B; Table 2; Supporting information Tables 1 and 3). The most electronegative region of **37** maps on the carboxyl group while that of **40** maps on the carbonyl oxygen of the benzoyl group (Figure 4A and B). Thus, even if one should exert caution against drawing conclusions from purely theoretical work, the QM calculations support our pharmacophoric hypothesis as to why **40** is inactive.

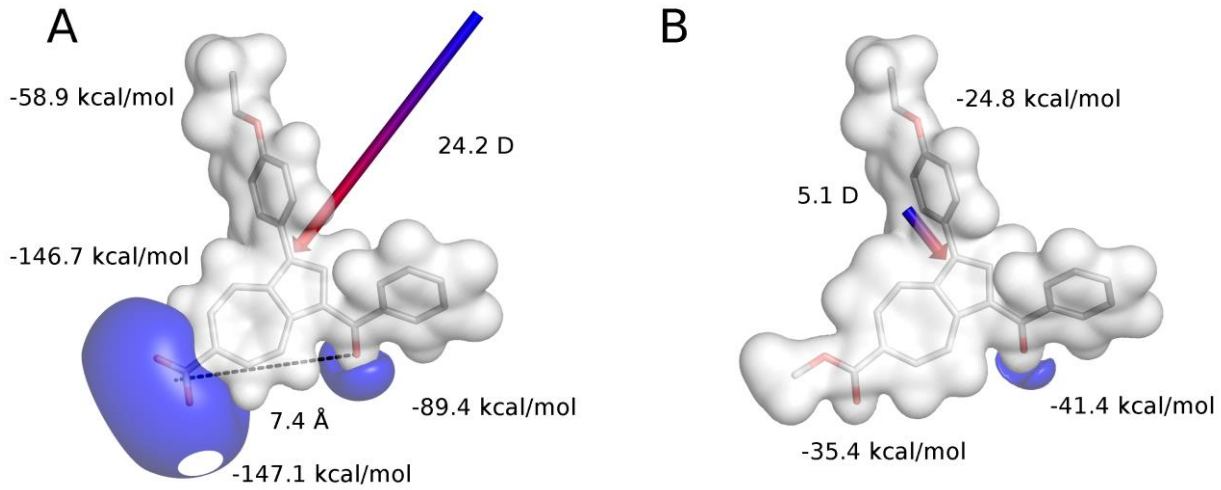

Figure 4. Electrostatic potential (ESP) surfaces of the weak agonist hit **37** (**A**) and its inactive ester analogue **40** (**B**). The arrows indicate the net dipole moments and the dashed lines mark the distance between the two most electron rich regions of the active compounds. The minimum ESP values on the molecular surface for each atom are indicated as kcal/mol.

Table 2. Minimum and maximum electrostatic potential values corresponding to the oxygen atoms at each hydrogen bond acceptor group of compounds **35**, **37**, **39** and **40**.

	R^1		R^3		R^6			
Compound	Min ESP (kcal/mol)	Max ESP (kcal/mol)	Min ESP (kcal/mol)	Max ESP (kcal/mol)	Min ESP (kcal/mol)	Max ESP (kcal/mol)	Min ESP (kcal/mol)	Max ESP (kcal/mol)
35	–37.8	–1.6	–31.7	6.9	–42.6	6.2	–19.8	3.1
37	–89.4	–56.0	–58.9	–40.1	–147.0	–93.0	–146.7	–92.7
39	–39.9	–5.7	–40.8	–2.4	–29.7	8.1	–3.5	17.6
40	–41.4	–5.3	–24.8	–1.7	–35.4	3.6	–10.5	13.8

Dipole moments

An assumption we made when choosing the azulene scaffold was that the presence of a dipole moment would be beneficial for the biological activity (as also hypothesized e.g. in reference[13]). In orexin receptors, the dipole moment would mimic the α-helical dipole of the endogenous peptide.[12,14] By itself the dipole moment of the azulene ring is small, in the order of a debye, and thus the functional groups attached would be the main drivers of the dipole moments of the azulene-scaffolded compounds. With active compounds identified, we have now the possibility to address this assumption.

As a result, the net dipole moment does not follow the distribution of charges on the unsubstituted azulene ring; instead, the presence of two or three main electronegative regions, notably the carboxyl/ester groups at the 6-position and carbonyl-containing groups at the 1-position, drive the strength and direction of the net dipole moments. In the azulene core alone the dipole moment is towards the five-membered ring, while in the indole core the electrons are localized mainly to the six-membered ring (Supporting information Figure 3). In this study both azulene and indole scaffolds yield active compounds though, as they allow the existence of equally electronegative regions within almost similar distance from each other despite of the differences in the scaffold (see compounds **35** and **39** in Figure 3C and Table 2).

*Comparison of the 1-benzoylazulenes to an orexin receptor agonist **41** (Nag26) and antagonists **42** (EMPA) and **43** (suvorexant)*

To investigate further whether the observed pharmacophoric signature of the active 1-benzoylazulenes is connected to orexin receptor activation, we studied **41**, the only currently reported and characterized orexin receptor agonist with full efficacy,[8,9] and antagonists **42** and **43** both co-crystallized in complex with OX_2 receptor.[31,32] It should be noted that until this point we have been considering effectors, which could act either selectively on OX_1 (the potentiator hits) or on both orexin receptor subtypes (weak agonists). However, **41** is 70-fold OX_2 selective, whereas antagonist **42** (EMPA) is 900-fold OX_2 selective. To simplify the discussion, and to avoid the misinterpretation of the data due to the subtype selectivity, from now on the discussion considers only compounds acting on OX_2 receptors (i.e. the known ligands **41**–**43**, which we compare to the weak agonist hits **1**, **2**, **26**, **28** and **37**).

The structure of agonist **41** is notably more extended and more flexible than those of our 1-benzoylazulene derivatives. As the electrostatic properties are conformation-specific, we needed first to investigate the conformational space of **41**. To accomplish this, we took advantage of sets of molecular dynamics (MD) simulations that we have conducted recently with **41** in complex with OX_2 receptor (8 μs in total)[33].

The MD data showed that the frequent locations of the sulphonamide group, the methoxyphenyl ring (so-called A-ring of the **41** molecule, see reference[8]) and the dimethylbenzamide ring remain relatively stable throughout the simulation, whereas the location of the methylbenzoyl ring (so-called B-ring) end of the molecule deviates more (Figure 5). The conformations of **41** observed along the trajectories could be grouped into three main clusters. The conformation of **41** in the representative pose of the largest cluster (Figure 5A and 5C) is C-shaped, whereas the second most occupied cluster represents the L-shaped **41** conformations (Figure 5B); the third cluster lies midway of the other two (Figure 5). When comparing the binding conformations of **41** in the MD trajectories to the crystal structure of orexin receptor antagonist **42** in complex with OX_2 receptor[31], Figure 5D), the location of the sulphonamide functionality of **42** aligns with the most frequent location of that of **41**. Additionally, the aromatic rings of **42** align with the ring locations of the **41** at the bottom of the binding site; however, **42** does not reach to the binding region of the B-ring of **41** (pink surfaces in Figure 5C–D).

As demonstrated in Figures 4 and 5 and Table 2, the electrostatic determinants of the agonist hit **37** resemble those of the representative **41** conformations highlighting that our 1-benzoylazulenes are actually similar to the A-ring-end of the compound **41** (both by their shape and their electrostatic properties; see also Supporting information Figure 2). The structure of **41** includes also a third electron-rich oxygen atom at the B-ring-end of the molecule. Since **41** is a relatively symmetrical (i.e. the shape and electrostatics of A-ring- and B-ring-ends of the **41** are highly similar; Figure 5A–B), the bound azulene derivatives could also overlap with the B-ring-end of **41**.

To compare **41** to **37** in the context of the receptor, we thus decided to study the binding mode of **37** using docking simulations. For docking we utilized OX_2 receptor (PDB ID: 5WQC[31]) under the assumption that **37** and **41** would bind to the same orthosteric binding site. Interestingly, the most populated binding mode of **37** indeed shows similarities to **41** in its interaction pattern (Figure 6 A–B). Both these compounds could form water-mediated hydrogen bonds with Gln134$^{3.32}$ (sulphonamide oxygen of **41** and carbonyl oxygen of **37**) and Thr231$^{5.46}$ (A-ring carbonyl of **41** and ethoxy oxygen of **37**). Additionally, the carbonyl group of the B-ring-end of **41** could hydrogen bond directly with Asn324$^{6.55}$, whereas the ethoxy oxygen of **37** is involved in this interaction via the same water molecule as in the interaction with Thr231$^{5.46}$. The carboxyl group of **37**, which superimposes on top of the B-ring carbonyl group of **41** (Figure 6C), could form a salt bridge with Arg328$^{6.59}$, while in **41**–OX_2-complex the Arg328$^{6.59}$ seems to be involved in π–cation

interaction with the π-electrons of the phenyl group of **41** (in the middle region of the molecule, next to the sulphonamide functionality). The lack of this salt bridge could also explain the complete loss of orexin receptor activation when changing the substituent at the 6-position of **37** to the corresponding methyl ester (compound **40**).

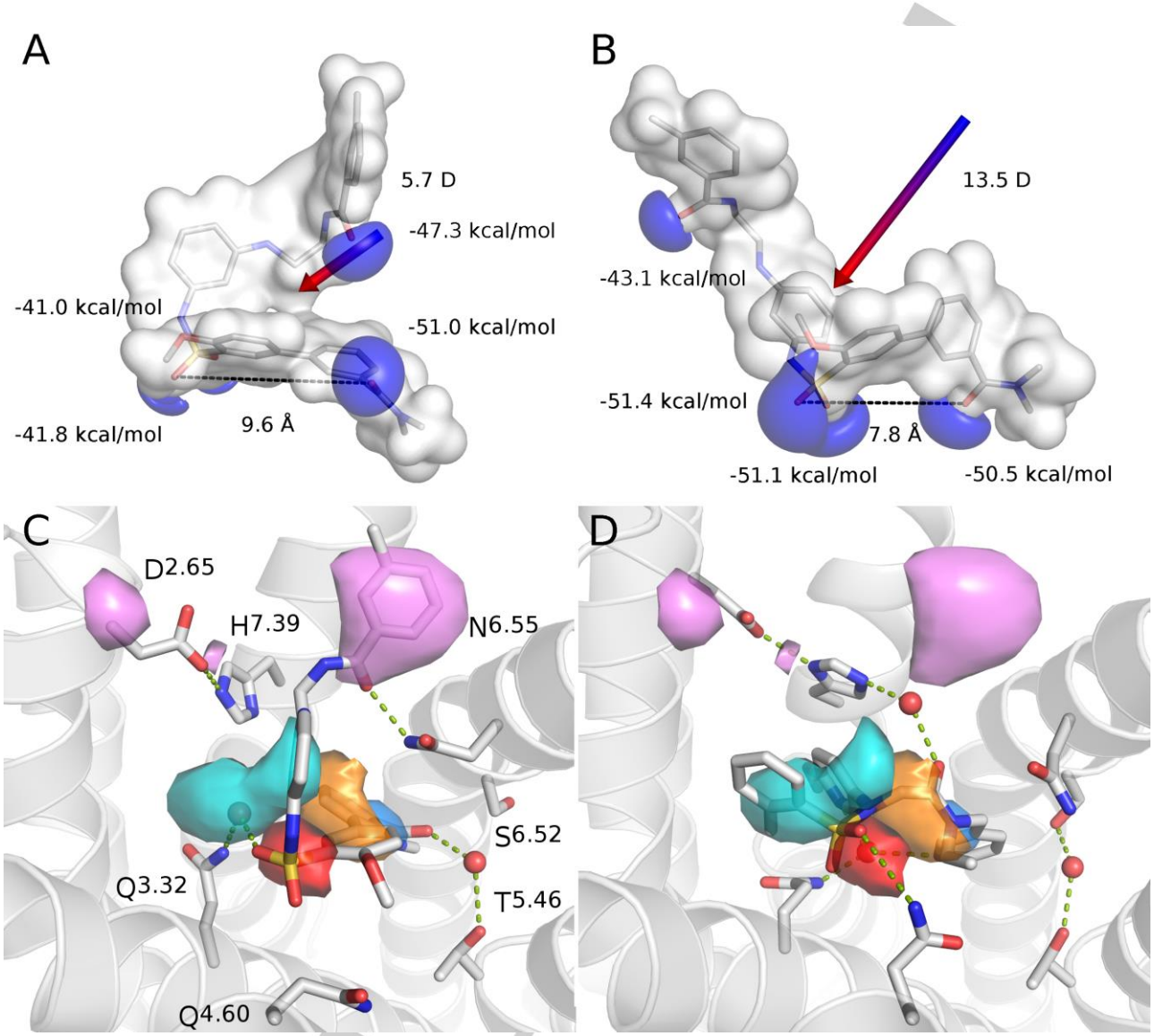

Figure 5. A. ESP surfaces of the poses of **41** representing the most (**A**) and second most (**B**) occupied conformation cluster across four MD simulation trajectories (8 µs in total). The arrows indicate the net dipole moments and the dashed lines mark the distance between the two most electron rich regions of the compounds. **C. 41** in complex with OX_2 receptor; the **41** pose is the same than the one presented in panel A. **D.** A crystal structure of an orexin receptor antagonist **42** (EMPA) in complex with OX_2 receptor (pdb ID: 5WQC). The surfaces indicate the most frequent locations of the four rings and the sulphonamide functionality of **41** throughout the simulation; pink corresponds to the location of the methylbenzoyl ring (B-ring in reference[8]), cyan the central benzene ring, red the sulphonamide group, orange the methoxyphenyl ring (A-ring), and cobalt blue the dimethylbenzamide ring. Red spheres represent water molecules and green dashes indicate possible hydrogen bonds. Carbon: white, oxygen: red, nitrogen: blue, sulphur: yellow. Only a subset of binding site water molecules and amino acid side chains are shown for clarity. The view is from the extracellular side of the receptor, behind TM4.

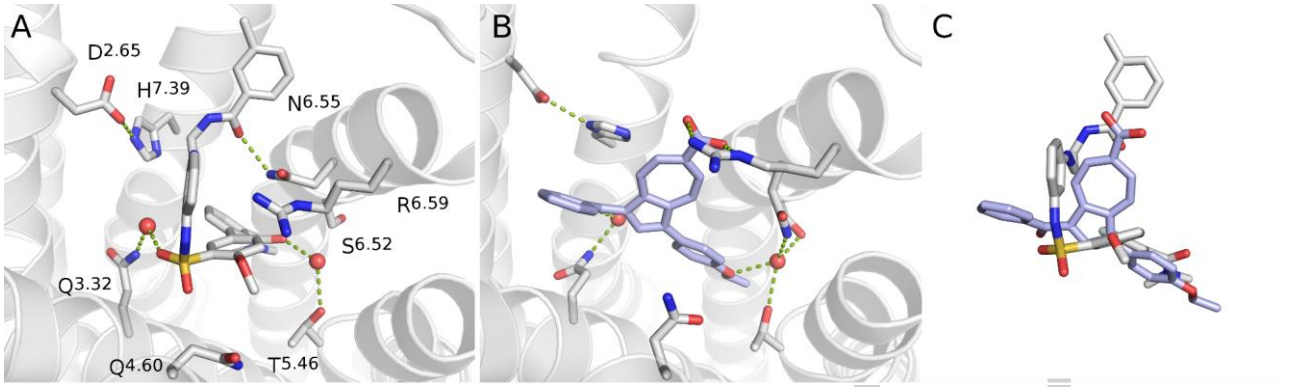

Figure 6. A. The representative pose of **41** as in Figure 5 C. **B.** A representative docking pose of **37** (representing the majority of the poses, 14/17, produced by Glide Induced Fit docking protocol). **C.** Superimposition of the poses presented in panels A and B. View and color code as in Figure 5.

We also considered the electrostatic potentials of the orexin receptor antagonists with sub-nanomolar binding affinities, the OX_2-selective **42** and dual **43** (suvorexant).[34–36] These antagonists lack the electron distribution characteristics that we suggest in this study for potentiators and weak agonists (Supporting Information Figure 4): the number and locations of the electronegative regions are different from those of the **41** and **37**. Additionally, the distances between the two strongest electronegative regions are shorter in the antagonist structures, 6.7 Å and 4.7 Å for **42** and **43**, respectively. When connecting this observation to the binding mode of **42**, the electron-rich region located on its pyridine ring does not reach as close to TMs 5 and 6 as the corresponding region of **41** (Figure 5). More generally, antagonist **42** lacks direct interactions with TMs 5 and 6. These findings support the hypothesis that the electronegative regions we have identified from the orexin receptor activating ligands would be involved in driving orexin receptor activation.

Conclusions

In this study we identified two azulene-based compounds, **26** and **28**, which act as weak orexin receptor agonists. These compounds showed concentration-dependent orexin receptor activation of a similar magnitude to their parent compound **1**. Additionally, we demonstrated the orexin receptor agonist activity of the previously reported compound **37**; the orexin receptor-specific maximum response obtained with **37** was approximately 18% of the E_{max} of orexin-A in both receptor subtypes. The SARs verified the importance of the 1-benzoylazulene scaffold, but could not elucidate the difference between agonist and potentiation hits suggesting an overlapping binding site. The active indole-based compounds demonstrated that the azulene ring *per se* is not required to make potentiators of the orexin system.

Together with the azulene SARs, the indoles highlighted the role of the spatial arrangement of the R-groups that led us to define a pharmacophore hypothesis (two hydrogen bond acceptors within 7-8 Å distance) that will guide further design. It should be noted that only few compounds have been tested that do not fit the pharmacophoric signature: two indole-scaffolded compounds in which the distance between the hydrogen bond acceptors has been shortened to ca. 5 Å lose their potentiation effect, in contrast to indoles with a longer distance between these acceptors. Compound **3** with only one hydrogen bond acceptor (4-trifluorobenzoyl at the 1-position, methyl at the 6-position; Figure 2) is neither a potentiator nor a weak agonist, but it inhibits [^{125}I]-orexin-A binding on both receptor subtypes.[12] Additionally, compounds with chloride at the 6-position were found to be inactive in terms of agonism, yet all seven of such compounds displaced [^{125}I]-orexin-A on OX_2 receptors.[12] There are also a few inactive compounds that do possess the reported pharmacophoric signature; this can be reconciled with the presence of otherwise unfitting substituents.

Apart from our compounds, similar electronegative regions were observed in the structure of the orexin receptor agonist **41** (but not the antagonist **43**). The MD and molecular docking studies, conducted under the assumption that azulene-based compounds bind to the orthosteric binding site of OX_2 receptors, propose that the electron-rich functional groups of **41** and the agonist hit **37** could interact with three separate regions at the binding pocket. In context of the binding mode of **41** (representing the most occupied conformation cluster in our MD simulation), these electron-rich areas are involved in interactions with Gln134$^{3.32}$ and Thr231$^{5.46}$. Additionally, a third electronegative region of **41** occupies a binding pocket in the vicinity of Arg328$^{6.59}$ above the orthosteric binding site. Of these sub-pockets, only the one close to Gln134$^{3.32}$ is occupied by orexin receptor antagonist **42**, suggesting that the other two might drive the orexin receptor activation.

Altogether, the data provided here (SARs, the indole-controlled shape assessment, and the computational results) should bring valuable insights to the design of potent azulene-based orexin receptor activators.

Experimental Section

Chemistry

General: All compounds were characterized by ^{1}H and ^{13}C NMR spectroscopy using a Bruker Avance III 400 MHz spectrometer. Chemical shifts are reported in parts per million (ppm) relative to the residual solvent signals: $CDCl_3$ 7.26 and 77.17 ppm, DMSO-d_6 2.50 and 39.52 ppm for ^{1}H and ^{13}C NMR, respectively. The progress of the reactions was monitored by thin-layer chromatography on silica gel 60-F_{254} plates. Silica gel (SiO_2)

60 (230−400 mesh) was used in flash chromatography purifications. Microwave reactions were performed in sealed reaction vessels using a Biotage Initiator+ instrument equipped with an external IR sensor to detect the reaction temperature. Mass spectrometric analysis were carried out with a Waters Synapt G2 HDMS mass spectrometer using electrospray ionization (ESI). Compound **14** was ionized with APPI/APCI ion source and its exact mass was corrected using testosterone as a lock-mass compound. The purity was determined by UPLC-MS with diode-array detector. The purity of the all biologically tested compounds was 95% or higher, except for **36** with 94% purity. ^{1}H NMR spectrum of **36** shows only hardly visible impurities.

General procedure for the synthesis of compounds 5–9: Compound **4** was dissolved in anhydrous 1,4-dioxane (0.70 mL) under argon. Appropriate acetamide derivative (4.3 equiv) and $POCl_3$ (4 equiv) were added. The resulting blue solution was heated under microwave irradiation at 100 °C for 2–5 h. The red reaction mixture was poured into a 1 M aqueous solution of NaOH (30 mL) on ice bath and extracted with DCM (25 + 15 mL). The organic phases were combined, washed with water (20 mL), dried over anhydrous Na_2SO_4, filtered, and evaporated to provide a crude product, which was purified by flash chromatography.

Methyl 1-(4-methoxybenzoyl)azulene-6-carboxylate (5): Compounds **4** (0.056 g, 0.30 mmol) and **40** (0.231 g, 1.29 mmol) with 4 h heating gave a dark green oil, which after flash chromatography (*n*-heptane/EtOAc 17:3) gave **5** as a green, amorphous solid (0.019 g, 22%). ^{1}H NMR (400 MHz, $CDCl_3$) δ 9.60 (d, J = 10.4 Hz, 1H), 8.56 (d, J = 10.4 Hz, 1H), 8.40 (dd, J = 10.4, 1.6 Hz, 1H), 8.29 (dd, J = 10.4, 1.6 Hz, 1H), 8.23 (d, J = 4.0 Hz, 1H), 7.89–7.86 (m, 2H), 7.38 (d, J = 4.4 Hz, 1H), 7.02–6.99 (m, 2H), 4.03 (s, 3H), 3.91 (s, 3H). ^{13}C NMR (101 MHz, $CDCl_3$) δ 191.6, 168.1, 162.7, 145.6, 144.6, 142.5, 138.1, 137.3, 136.9, 133.5, 132.1, 128.6, 126.9, 126.6, 118.4, 113.6, 55.6, 53.5. HRMS (ESI-QTOF) *m/z*: [M + H]$^+$ Calcd for $C_{20}H_{17}O_4$ 321.1127; Found 321.1127.

Methyl 1-(3-methoxybenzoyl)azulene-6-carboxylate (6): Compounds **4** (0.056 g, 0.30 mmol) and **41** (0.231 g, 1.29 mmol) with 5 h heating gave a dark brown solid, which after flash chromatography (*n*-heptane/EtOAc 17:3) gave **6** as a green, amorphous solid (0.016 g, 18%). ^{1}H NMR (400 MHz, $CDCl_3$) δ 9.71 (d, J = 10.4 Hz, 1H), 8.56 (d, J = 10.0 Hz, 1H), 8.45 (dd, J = 10.4 Hz, 1.6 Hz, 1H), 8.32 (dd, J = 10.4, 1.6 Hz, 1H), 8.23 (d, J = 4.0 Hz, 1H), 7.43–7.38 (m, 3H), 7.36 (d, J = 4.0 Hz, 1H), 7.14–7.11 (m, 1H), 4.04 (m, 3H), 3.88 (m, 3H). ^{13}C NMR (101 MHz, $CDCl_3$) δ 192.5, 168.0, 159.7, 146.1, 145.2, 142.8, 142.3, 138.2, 137.5, 137.0, 129.3, 129.2, 127.4, 125.9, 122.4, 118.6, 117.9, 114.2, 55.6, 53.5. HRMS (ESI-QTOF) *m/z*: [M + H]$^+$ Calcd for $C_{20}H_{17}O_4$ 321.1127; Found 321.1127.

Methyl 1-[3-(methoxycarbonyl)benzoyl]azulene-6-carboxylate (7): Compounds **4** (0.056 g, 0.30 mmol) and **42** (0.267 g, 1.29 mmol) with 5 h heating gave a dark blueish oil, which after two flash chromatography purifications (*n*-heptane/EtOAc 17:3 and DCM/EtOAc 24:1) gave **7** as a green, amorphous solid (0.038 g, 44%). ^{1}H NMR (400 MHz, $CDCl_3$) δ 9.75 (d, J = 10.4 Hz, 1H), 8.59 (d, J = 10.4 Hz, 1H), 8.50–8.47 (m, 2H), 8.34 (dd, J = 10.4, 1.6 Hz, 1H), 8.25 (dt, J = 8.0, 1.6 Hz, 1H), 8.16 (d, J = 4.4 Hz, 1H), 8.05 (dt, J = 7.6, 1.6 Hz, 1H), 7.60 (t, J = 7.8 Hz, 1H), 7.37 (d, J = 4.0 Hz, 1H), 4.04 (s, 3H), 3.94 (s, 3H). ^{13}C NMR (101 MHz, $CDCl_3$) δ 191.7, 167.9, 166.7, 146.3, 145.1, 143.0, 141.4, 138.4, 137.7, 137.2, 133.8, 132.4, 130.7, 130.4, 129.5, 128.7, 127.7, 125.4, 118.9, 53.6, 52.5. HRMS (ESI-QTOF) *m/z*: [M + H]$^+$ Calcd for $C_{21}H_{17}O_5$ 349.1076; Found 349.1078.

Methyl 1-(2-phenylacetyl)azulene-6-carboxylate (8): Compounds **4** (0.056 g, 0.30 mmol) and **43** (0.211 g, 1.29 mmol) with 5 h heating gave a dark brown oil, which after flash chromatography (*n*-heptane/EtOAc 17:3) gave **8** as a lime green, amorphous solid (0.028 g, 31%). ^{1}H NMR (400 MHz, $CDCl_3$) δ 9.93 (d, J = 10.4, 1H), 8.51 (d, J = 10.4 Hz, 1H), 8.49 (d, J = 4.4 Hz, 1H), 8.41 (dd, J = 10.4, 1.6 Hz, 1H), 8.28 (dd, J = 10.4, 1.6 Hz, 1H), 7.38–7.31 (m, 5H), 7.27–7.22 (m, 1H), 4.38 (s, 2H), 4.02 (s, 3H). ^{13}C NMR (101 MHz, $CDCl_3$) δ 195.0, 167.9, 146.1, 143.1, 142.2, 138.3, 138.2, 137.1, 135.8, 129.7, 129.6, 128.8, 127.5, 126.8, 125.1, 118.9, 53.5, 48.3. HRMS (ESI-QTOF) *m/z*: [M + H]$^+$ Calcd for $C_{20}H_{17}O_3$ 305.1178; Found 305.1178.

Methyl 1-(thiophene-2-carbonyl)azulene-6-carboxylate (9): Compounds **4** (0.056 g, 0.30 mmol) and **44** (0.189 g, 1.29 mmol) with 5 h heating gave a dark green oil, which after flash chromatography (*n*-heptane/EtOAc 17:3) gave **9** as a green, amorphous solid (0.026 g, 29%). ^{1}H NMR (400 MHz, $CDCl_3$) δ 9.63 (d, J = 10.4 Hz, 1H), 8.58 (d, J = 10.4 Hz, 1H), 8.50 (d, J = 4.0 Hz, 1H), 8.42 (dd, J = 10.4, 1.6 Hz, 1H), 8.31 (dd, J = 10.4, 1.6 Hz, 1H), 7.74 (dd, J = 3.8, 1.0 Hz, 1H), 7.69 (dd, J = 5.2, 1.2 Hz, 1H), 7.41 (d, J = 4.0 Hz, 1H), 7.20 (dd, J = 4.8, 3.6 Hz, 1H), 4.04 (s, 3H). ^{13}C NMR (101 MHz, $CDCl_3$) δ 183.6, 168.0, 146.5, 145.7, 143.4, 142.5, 138.3, 137.3, 137.1, 133.2, 132.7, 128.8, 127.9, 127.1, 126.0, 118.7, 53.49. HRMS (ESI-QTOF) *m/z*: [M + H]$^+$ Calcd for $C_{17}H_{13}O_3S$ 297.0585; Found 297.0586.

Methyl 1-chloro-3-(thiophene-2-carbonyl)azulene-6-carboxylate (10): ^{1}H NMR (400 MHz, $CDCl_3$) δ 9.56 (d, J = 10.4 Hz, 1H), 8.61 (d, J = 10.4 Hz, 1H), 8.39 (dd, J = 10.4, 1.2 Hz, 1H), 8.35 (s, 1H), 8.32 (dd, J = 10.6, 1.4 Hz, 1H), 7.74–7.70 (m, 2H), 7.21 (dd, J = 5.0, 3.8 Hz, 1H), 4.04 (s, 3H). ^{13}C NMR (101 MHz, $CDCl_3$) δ 182.6, 167.6, 146.0, 141.1, 140.6, 139.5, 138.8, 138.2, 134.9, 133.4, 133.2, 129.3, 128.0, 127.1, 123.7, 118.2, 53.65. HRMS (ESI-QTOF) *m/z*: [M + H]$^+$ Calcd for $C_{17}H_{12}O_3SCl$ 331.0196; Found 331.0196.

Methyl 1-(2-chloroacetyl)azulene-6-carboxylate (12): Compounds **4** (0.056 g, 0.30 mmol) and 2-chloro-*N,N*-diethylacetamide (0.18 mL, 1.29 mmol) with 2 h heating gave a dark brown oil, which after flash chromatography (manual gradient of *n*-heptane/EtOAc 17:3 → 3:1) gave **12** as a green, amorphous solid (0.026 g, 33%). ^{1}H NMR (400 MHz, $CDCl_3$) δ 9.90 (d, J = 10.4 Hz, 1H), 8.57 (d, J = 10.4 Hz, 1H), 8.49 (dd, J = 10.4, 1.6 Hz, 1H), 8.39 (d, J = 4.0 Hz, 1H), 8.35 (dd, J = 10.4, 1.6 Hz, 1H), 7.36 (d, J = 4.0 Hz, 1H), 4.76 (s, 2H), 4.04 (s, 3H). ^{13}C NMR (101 MHz, $CDCl_3$) δ 187.8, 167.7, 146.5, 142.7, 142.2, 138.7, 138.3, 137.4, 130.3, 128.3, 122.4, 119.3, 53.60, 47.53. HRMS (ESI-QTOF) *m/z*: [M + H]$^+$ Calcd for $C_{14}H_{12}O_3Cl$ 263.0475; Found 263.0475.

Methyl 1-(2-methylthiazol-4-yl)azulene-6-carboxylate (13): Compound **12** (0.026 g, 0.10 mmol) and thioacetamide (0.015 g, 0.20 mmol) were suspended in EtOH under argon. The resulting blue suspension was heated under microwave irradiation at 120 °C for 30 min. The green solution was diluted with DCM (20 mL) and washed with a 1 M aqueous solution of NaOH (15 mL), water (10 mL) and brine (10 mL), dried over anhydrous Na_2SO_4, filtered and evaporated to provide a green solid. The crude product was purified by flash chromatography (*n*-heptane/EtOAc 4:1) to give **13** as a green, amorphous solid (0.020 g, 71%). ^{1}H NMR (400 MHz, $CDCl_3$) δ 9.36 (d, J = 10.4 Hz, 1H), 8.35 (d, J = 10.0 Hz, 1H), 8.32 (d, J = 4.0 Hz, 1H), 8.06 (d, J = 10.4, 1.6 Hz, 1H), 8.00 (d, J = 9.8, 1.4 Hz, 1H), 7.44 (d, J = 4.0 Hz, 1H), 7.30 (s, 1H), 3.99 (s, 3H), 2.85 (s, 3H). ^{13}C NMR (101 MHz, $CDCl_3$) δ 168.7, 165.7, 152.0, 143.8, 139.8, 137.1, 136.0, 135.6, 135.5, 124.6, 124.2, 123.9, 118.8, 113.0, 53.2, 19.6. HRMS (ESI-QTOF) *m/z*: [M + H]$^+$ Calcd for $C_{16}H_{14}NO_2S$ 284.0745; Found 284.0747.

Methyl 1-(2-amino-2-oxoacetyl)azulene-6-carboxylate (14): Oxalyl chloride (0.019 mL, 0.23 mmol) was added dropwise to a solution of **4** (0.028 g, 0.15 mmol) in anhydrous toluene (0.90 mL) under argon. The resulting mixture was stirred at room temperature for 1 h and the solvents were evaporated. The residue was dissolved in anhydrous DCM (0.90 mL) under argon. The solution was cooled to 0 °C and a 7 M solution of NH_3 in MeOH (0.064 mL, 0.45 mmol) was added. The green suspension was stirred at 0 °C for 10 min. The reaction mixture was diluted with DCM (25 mL) and it was washed with water (3 × 10 mL), dried over anhydrous Na_2SO_4, filtered and evaporated to provide a green solid. The crude product was purified by flash chromatography (manual gradient of DCM → DCM/MeOH 19:1) to give **14** as a green, amorphous solid (0.025 g, 64%) ^{1}H NMR (400 MHz, DMSO-d_6) δ 9.75 (d, J = 10.0 Hz, 1H), 8.84 (d, J = 10.4 Hz, 1H), 8.71 (d, J = 4.0 Hz, 1H), 8.48 (d, J = 10.4 Hz, 1H), 8.35 (d, J = 10.0 Hz, 1H), 8.20 (s, 1H), 7.82 (s, 1H), 7.53 (d, J = 4.0 Hz, 1H), 3.98 (s,

3H). ^{13}C NMR (101 MHz, DMSO-d_6) δ 186.1, 167.4, 167.1, 146.5, 145.8, 142.5, 138.3, 138.0, 136.9, 129.9, 128.5, 121.1, 120.0, 53.5. HRMS (APPI/APCI-QTOF) *m/z*: $[M + H]^+$ Calcd for $C_{14}H_{12}NO_4$ 258.0766; Found 258.0764.

Methyl 1-[2-oxo-2-(phenylamino)acetyl]azulene-6-carboxylate (15): Oxalyl chloride (0.019 mL, 0.23 mmol) was added dropwise to a solution of **4** (0.028 g, 0.15 mmol) in anhydrous toluene (0.90 mL) under argon. The resulting mixture was stirred at room temperature for 1 h and the solvents were evaporated. The residue was dissolved in anhydrous DCM (0.90 mL) under argon and aniline (0.055 mL, 0.60 mmol) was added. The reaction mixture was stirred at room temperature for 30 min. The reaction mixture was diluted with DCM (25 mL) and it was washed with a 1 M aqueous solution of HCl (15 mL), a saturated aqueous solution of $NaHCO_3$ (15 mL) and water (15 mL), dried over anhydrous Na_2SO_4, filtered and evaporated to provide a green solid. The crude product was purified by flash chromatography (manual gradient of *n*-heptane/DCM 2:3 → DCM) to give **15** as a green, amorphous solid (0.025 g, 50%). ^{1}H NMR (400 MHz, $CDCl_3$) δ 9.88 (d, J = 10.4 Hz, 1H), 9.43 (d, J = 4.0 Hz, 1H), 9.33 (s, 1H), 8.57–8.53 (m, 2H), 8.40 (d, J = 10.0 Hz, 1H), 7.77–7.74 (m, 2H), 7.43–7.38 (m, 3H), 7.21–7.17 (m, 1H), 4.04 (s, 3H). ^{13}C NMR (101 MHz, $CDCl_3$) δ 181.7, 167.6, 160.7, 147.9, 145.5, 138.4, 137.5, 137.2, 137.0, 131.1, 129.3, 129.3, 125.1, 121.6, 120.7, 112.0, 53.61. HRMS (ESI-QTOF) *m/z*: $[M + H]^+$ Calcd for $C_{20}H_{16}NO_4$ 334.1079; Found 334.1074.

Methyl 1-carbamoylazulene-6-carboxylate (16): A 20% solution of phosgene in toluene (0.53 mL, 1.0 mmol) was added to a solution of **4** (0.037 g, 0.20 mmol) in anhydrous toluene (0.50 mL) under argon. The resulting blue mixture was stirred at 80 °C for 17 h and the solvents were evaporated. The residue was dissolved in anhydrous DCM (1.2 mL) and the solution was cooled with ice bath. A 7 M solution of NH_3 in MeOH (0.14 mL, 1.0 mmol) was added. The blue reaction mixture was stirred at 0 °C for 30 min and then it was diluted with DCM (30 mL). The organic phase was washed with a 1 M aqueous solution of HCl (15 mL), a saturated aqueous solution of $NaHCO_3$ (15 mL) and water (15 mL), dried over anhydrous Na_2SO_4, filtered and evaporated to provide a blue oil. The crude product was purified by flash chromatography (manual gradient of EtOAc → EtOAc/MeOH 19:1) to give **16** as a blue, amorphous solid (0.016 g, 35%). ^{1}H NMR (400 MHz, DMSO-d_6) δ 9.78 (d, J = 10.8 Hz, 1H), 8.67 (d, J = 10.0 Hz, 1H), 8.53 (d, J = 4.0 Hz, 1H), 8.19 (dd, J = 10.8, 1.6 Hz, 1H), 8.13 (dd, J = 10.0, 1.6 Hz, 1H), 7.90 (s, 1H), 7.47 (d, J = 4.4 Hz, 1H), 7.21 (s, 1H), 3.96 (s, 3H). ^{13}C NMR (101 MHz, DMSO-d_6) δ 167.6, 166.7, 143.8, 140.6, 139.8, 137.2, 136.8, 136.3, 125.7, 125.2, 121.7, 118.0, 53.3. HRMS (ESI-QTOF) *m/z*: $[M + H]^+$ Calcd for $C_{13}H_{12}NO_3$ 230.0817; Found 230.0818.

Dimethyl azulene-1,6-dicarboxylate (17): The above-described reaction gave the side product **17** as a blue, amorphous solid (0.008 g, 9%). ^{1}H NMR (400 MHz, $CDCl_3$) δ 9.68 (d, J = 10.4 Hz, 1H), 8.51 (d, J = 10.0 Hz, 1H), 8.48 (d, J = 4.0 Hz, 1H), 8.38 (dd, J = 10.8, 1.6 Hz, 1H), 8.27 (dd, J = 10.0, 1.6 Hz, 1H), 7.35 (d, J = 4.0 Hz, 1H), 4.03 (s, 3H), 3.97 (s, 3H). ^{13}C NMR (101 MHz, $CDCl_3$) δ 168.1, 165.6, 145.9, 143.2, 141.9, 137.7, 136.7, 136.3, 127.8, 126.9, 118.6, 117.9, 53.5, 51.4. HRMS (ESI-QTOF) *m/z*: $[M + H]^+$ Calcd for $C_{14}H_{13}O_4$ 245.0814; Found 245.0813.

Methyl 1-(phenylcarbamoyl)azulene-6-carboxylate (19): The same procedure as described above was repeated with trimethylamine (0.056 mL, 0.40 mmol) and aniline (0.091 mL, 1.0 mmol) instead of NH_3 in MeOH to provide a green solid, which was purified by flash chromatography (manual gradient of DCM → DCM/EtOAc 23:2) to give **19** as a green, amorphous solid (0.051 g, 84%). ^{1}H NMR (400 MHz, $CDCl_3$) δ 9.78 (d, J = 10.8 Hz, 1H), 8.53 (d, J = 10.4 Hz, 1H), 8.33 (dd, J = 10.4, 1.6 Hz, 1H), 8.26–8.23 (m, 2H), 7.84 (s, 1H), 7.70–7.68 (m, 2H), 7.43–7.38 (m, 3H), 7.18–7.14 (m, 1H), 4.03 (s, 3H). ^{13}C NMR (101 MHz, $CDCl_3$) δ 168.1, 163.9, 144.8, 141.0, 138.5, 138.1, 137.1, 136.9, 129.2, 127.3, 126.2, 124.3, 121.7, 120.3, 118.1, 53.44. HRMS (ESI-QTOF) *m/z*: $[M + H]^+$ Calcd for $C_{19}H_{16}NO_3$ 306.1130; Found 306.1129.

Methyl 1-(dimethylcarbamoyl)azulene-6-carboxylate (18): A 20% solution of phosgene in toluene (0.12 mL, 0.23 mmol) was added to a solution of **4** (0.028 g, 0.15 mmol) in anhydrous toluene (0.70 mL) under argon. The resulting blue mixture was stirred at 60 °C for 18 h and then phosgene in toluene (20%, 0.20 mL, 0.38 mmol) was added. The heating was continued at 80 °C for 5 h. The reaction mixture was cooled with ice bath and a 2 M solution of dimethylamine in THF (0.75 mL, 1.5 mmol) was added. The resulting mixture was stirred at 0 °C for 15 min and then it was diluted with DCM (25 mL). The organic phase was washed with a 1 M aqueous solution of NaOH (15 mL), a 1 M aqueous solution of HCl (25 mL) and water (25 mL), dried over anhydrous Na_2SO_4, filtered and evaporated to provide a blue solid. The crude product was purified by flash chromatography (EtOAc) to give **18** as a turquoise, amorphous solid (0.019 g, 49%). ^{1}H NMR (400 MHz, $CDCl_3$) δ 8.77 (d, J = 10.4 Hz, 1H), 8.45 (d, J = 10.0 Hz, 1H), 8.17–8.13 (m, 2H), 8.06 (d, J = 4.0 Hz, 1H), 7.38 (d, J = 4.0 Hz, 1H), 4.00 (s, 3H), 3.15 (s, 6H). ^{13}C NMR (101 MHz, $CDCl_3$) δ 168.6, 168.4, 143.2, 139.8, 139.0, 137.3, 136.2, 135.3, 125.2, 125.1, 124.1, 117.8, 53.3, 37.7. HRMS (ESI-QTOF) *m/z*: $[M + H]^+$ Calcd for $C_{15}H_{16}NO_3$ 258.1130; Found 258.1135.

General procedure for the synthesis of compounds 21–26: A 0.25 M solution of **20** in anhydrous DMF was cooled to 0 °C and EDC·HCl (1.1 equiv) and HOBt·H_2O (1.1 equiv) were added. The resulting blue reaction mixture was stirred at 0 °C for 15 min and at room temperature for 1 h. Appropriate amine derivative (2.5 equiv) was added and stirring was continued at room temperature for an additional 1–2.5 h. Water (15 mL, for **21**, **22**, **25**, **26**) or a saturated solution of $NaHCO_3$ (15 mL, for **23**, **24**) was added to the purple mixture and it was extracted with EtOAc (30 mL). The organic phase was washed with a 1 M aqueous solution of HCl (15 mL, for **21**, **22**, **25**) and a saturated solution of $NaHCO_3$ (15 mL, two times for **23**, **24**, **26**), dried over anhydrous Na_2SO_4, filtered and evaporated to provide a crude product, which was purified by flash chromatography.

1-Benzoyl-*N*-methylazulene-6-carboxamide (21): Compound **20** (0.069 g, 0.25 mmol) and $MeNH_2$ in EtOH (33%, 0.082 mL, 0.63 mmol) gave a green-blue solid, which after flash chromatography (EtOAc) gave **21** as a green, amorphous solid (0.057 g, 79%). ^{1}H NMR (400 MHz, DMSO-d_6) δ 9.59 (d, J = 10.0 Hz, 1H), 8.82 (q, J = 4.4 Hz, 1H), 8.79 (d, J = 10.4 Hz, 1H), 8.12 (d, J = 4.0 Hz, 1H), 8.05 (dd, J = 10.2, 1.4 Hz, 1H), 7.97 (dd, J = 10.0, 1.6 Hz, 1H), 7.79–7.77 (m, 2H), 7.66–7.62 (m, 1H), 7.58–7.54 (m, 2H), 7.48 (d, J = 4.0 Hz, 1H), 2.86 (d, J = 4.4 Hz, 3H). ^{13}C NMR (101 MHz, DMSO-d_6) δ 191.5, 168.8, 145.4, 144.7, 143.3, 140.9, 140.5, 138.4, 137.5, 131.5, 129.1, 128.4, 127.3, 126.4, 124.5, 118.6, 26.83. HRMS (ESI-QTOF) *m/z*: $[M + H]^+$ Calcd for $C_{19}H_{16}NO_2$ 290.1181; Found 290.1183.

1-Benzoyl-*N*-(2-hydroxyethyl)azulene-6-carboxamide (22): Compound **20** (0.069 g, 0.25 mmol) and ethanolamine (0.038 mL, 0.63 mmol) gave a green-blue solid, which after flash chromatography (EtOAc/MeOH 19:1) gave **22** as a green, amorphous solid (0.068 g, 85%).^{1}H NMR (400 MHz, DMSO-d_6) δ 9.59 (d, J = 10.4 Hz, 1H), 8.84 (t, J = 5.6 Hz, 1H), 8.80 (d, J = 10.4 Hz, 1H), 8.12 (d, J = 4.4 Hz, 1H), 8.07 (dd, J = 10.4, 1.6 Hz, 1H), 7.98 (dd, J = 10.0, 1.6 Hz, 1H), 7.80–7.77 (m, 2H), 7.67–7.62 (m, 1H), 7.59–7.55 (m, 2H), 7.49 (d, J = 4.0 Hz, 1H), 4.81 (t, J = 5.6 Hz, 1H), 3.58 (q, J = 5.9 Hz, 2H), 3.40 (q, J = 6.0 Hz, 2H). ^{13}C NMR (101 MHz, DMSO-d_6) δ 191.5, 168.6, 145.6, 144.7, 143.3, 140.9, 140.5, 138.4, 137.5, 131.5, 129.1, 128.4, 127.4, 126.6, 124.5, 118.6, 59.6, 42.8. HRMS (ESI-QTOF) *m/z*: $[M + H]^+$ Calcd for $C_{20}H_{18}NO_3$ 320.1287; Found 320.1287.

(1-Benzoylazulen-6-yl)(4-methylpiperazin-1-yl)methanone (23): Compound **20** (0.069 g, 0.25 mmol) and 1-methylpiperazine (0.070 mL, 0.63 mmol) gave a purple solid, which after flash chromatography (EtOAc/EtOH/Et_3N 74:24:2) gave **23** as a purple, amorphous solid (0.079 g, 88%). ^{1}H NMR (400 MHz, DMSO-d_6) δ 9.58 (d, J = 10.4 Hz, 1H), 8.76 (d, J = 10.0 Hz, 1H), 8.10 (d, J = 4.0 Hz, 1H), 7.79–7.76 (m, 2H), 7.68–7.63 (m, 2H), 7.59–7.55 (m, 3H), 7.50 (d, J = 4.0 Hz, 1H), 3.71–3.68 (m, 2H), 3.27–3.24 (m, 2H), 2.46–2.43 (m, 2H), 2.31–2.28 (m, 2H), 2.22 (s, 3H). ^{13}C NMR (101 MHz, DMSO-d_6) δ 191.6, 169.0, 147.2, 144.1, 142.8, 140.5, 140.3, 139.3, 138.3, 131.5, 129.1, 128.4, 126.6, 125.7, 124.8, 118.9,

54.4, 54.1, 46.9, 45.5, 41.4. HRMS (ESI-QTOF) *m/z*: $[M + H]^+$ Calcd for $C_{23}H_{23}N_2O_2$ 359.1760; Found 359.1760.

***N*-[2-(1H-Imidazol-5-yl)ethyl]-1-benzoylazulene-6-carboxamide (24):** Compound **20** (0.069 g, 0.25 mmol) and histamine (0.070 g, 0.63 mmol) gave a dark green solid, which after flash chromatography (EtOAc/EtOH/Et_3N 74:24:2) gave **24** as a dark grey, amorphous solid (0.045 g, 49%). ^1H NMR (400 MHz, DMSO-d_6) δ 11.86 (s, 1H), 9.59 (d, J = 10.4 Hz, 1H), 8.94 (t, J = 5.6 Hz, 1H), 8.80 (d, J = 10.0 Hz, 1H), 8.13 (d, J = 4.0 Hz, 1H), 8.04 (dd, J = 10.2, 1.4 Hz, 1H), 7.95 (dd, J = 10.4, 1.6 Hz, 1H), 7.80–7.77 (m, 2H), 7.67–7.63 (m, 1H), 7.59–7.55 (m, 3H), 7.49 (d, J = 4.0 Hz, 1H), 6.88 (s, 1H), 3.57–3.52 (m, 2H), 2.82 (t, J = 7.4 Hz, 2H). ^{13}C NMR (101 MHz, DMSO-d_6) δ 191.5, 168.4, 145.7, 144.7, 143.3, 140.9, 140.5, 138.5, 137.5, 134.8, 131.5, 129.1, 128.4, 127.3, 126.5, 124.5, 118.6, 40.0. HRMS (ESI-QTOF) *m/z*: $[M + H]^+$ Calcd for $C_{23}H_{20}N_3O_2$ 370.1555; Found 370.1559.

***N*-[2-(1*H*-indol-3-yl)ethyl]-1-benzoylazulene-6-carboxamide (25):** Compound **20** (0.036 g, 0.13 mmol) and tryptamine (0.053 g, 0.33 mmol) gave a purple oil, which after flash chromatography (EtOAc) gave **25** as a dark grey, amorphous solid (0.044g, 81%). ^1H NMR (400 MHz, DMSO-d_6) δ 10.85 (s, 1H), 9.59 (d, J = 10.4 Hz, 1H), 8.99 (t, J = 5.6 Hz, 1H), 8.79 (d, J = 10.0 Hz, 1H), 8.13 (d, J = 4.0 Hz, 1H), 8.03 (d, J = 10.4 Hz, 1H), 7.96 (d, J = 10.0 Hz, 1H), 7.80–7.77 (m, 2H), 7.66–7.55 (m, 4H), 7.49 (d, J = 4.0 Hz, 1H), 7.36 (d, J = 8.0 Hz, 1H). 7.24 (s, 1H), 7.08 (t, J = 7.4 Hz, 1H), 7.00 (t, J = 7.4 Hz, 1H), 3.64–3.59 (m, 2H), 3.03 (t, J = 7.4 Hz, 2H). ^{13}C NMR (101 MHz, DMSO-d_6) δ 191.5, 168.4, 145.7, 144.7, 143.3, 140.9, 140.5, 138.4, 137.5, 136.3, 131.5, 129.1, 128.4, 127.4, 127.3, 126.5, 124.5, 122.8, 121.0, 118.6, 118.3, 111.7, 111.4, 40.9, 24.95. HRMS (ESI-QTOF) *m/z*: $[M + H]^+$ Calcd for $C_{28}H_{23}N_2O_2$ 419.1760; Found 419.1756.

1-Benzoyl-*N*-(pyridin-3-ylmethyl)azulene-6-carboxamide (26): Compound **20** (0.069 g, 0.25 mmol) and 3-picolylamine (0.064 mL, 0.63 mmol) gave a green solid, which after flash chromatography (EtOAc/MeOH 49:1) gave **26** as a green, amorphous solid (0.074 g, 80%). ^1H NMR (400 MHz, DMSO-d_6) δ 9.60 (d, J = 10.4 Hz, 1H), 9.48 (t, J = 5.8 Hz, 1H), 8.81 (d, J = 10.4 Hz, 1H), 8.63 (d, J = 1.6 Hz, 1H), 8.50 (dd, J = 4.8, 1.6 Hz, 1H), 8.14 (d, J = 4.0 Hz, 1H), 8.11 (dd, J = 10.4, 1.6 Hz, 1H), 8.01 (dd, J = 10.2, 1.4 Hz, 1H), 7.83–7.77 (m, 3H), 7.66–7.62 (m, 1H), 7.59–7.54 (m, 2H), 7.50 (d, J = 4.0 Hz, 1H), 7.40 (dd, J = 8.0, 4.8 Hz, 1H), 4.57 (d, J = 6.0 Hz, 2H). ^{13}C NMR (101 MHz, DMSO-d_6) δ 191.5, 168.7, 148.9, 148.3, 145.0, 144.7, 143.4, 141.0, 140.5, 138.5, 137.5, 135.3, 134.6, 131.5, 129.1, 128.4, 127.4, 126.4, 124.6, 123.6, 118.7, 41.1. HRMS (ESI-QTOF) *m/z*: $[M + H]^+$ Calcd for $C_{24}H_{19}N_2O_2$ 367.1447; Found 367.1446.

1-(3-Methoxybenzoyl)azulene-6-carboxylic acid (27): Compound **6** (0.11 g, 0.34 mmol) was dissolved in THF (3 mL) and MeOH (0.5 mL). A 2 M aqueous solution of NaOH (0.5 mL) was added to the blue solution and the resulting mixture was stirred at room temperature for 30 min. A 1 M aqueous solution of HCl (5 mL) was added to the purple reaction mixture on ice bath and then the mixture was extracted with EtOAc (40 mL). The organic phase was washed with a 1 M aqueous solution of HCl (2 × 20 mL) and brine (20 mL), dried over anhydrous Na_2SO_4, filtered and evaporated to provide a green solid. The crude product was purified by flash chromatography (manual gradient of EtOAc/AcOH 99:1) to give **27** as a green, amorphous solid (0.10 g, 98%). ^1H NMR (400 MHz, DMSO-d_6) δ 9.61 (d, J = 10.4 Hz, 1H), 8.82 (d, J = 10.4 Hz, 1H), 8.44 (dd, J = 10.4, 1.6 Hz, 1H), 8.33 (dd, J = 10.4, 1.6 Hz, 1H), 8.21 (d, J = 4.4 Hz, 1H), 7.52 (d, J = 4.0 Hz, 1H), 7.48 (t, J = 8.0 Hz, 1H), 7.34–7.32 (m, 1H), 7.30–7.29 (m, 1H), 7.23–7.20 (m, 1H), 3.83 (s, 3H). ^{13}C NMR (101 MHz, DMSO-d_6) δ 191.2, 168.3, 159.1, 145.4, 144.4, 141.8, 141.7, 139.5, 138.0, 137.0, 129.5, 128.9, 127.6, 124.7, 121.6, 118.8, 117.5, 113.9, 55.3. HRMS (ESI-QTOF) *m/z*: $[M - H]^-$ Calcd for $C_{19}H_{13}O_4$ 305.0814; Found 305.0813.

***N*-(2-Hydroxyethyl)-1-(3-methoxybenzoyl)azulene-6-carboxamide (28):** Compound **27** (0.046 g, 0.15 mmol) was dissolved in DMF (1 mL). The blue solution was cooled to 0 °C and EDC-HCl (0.032 g, 0.17 mmol) and HOBt-H_2O (0.025 g, 0.17 mmol) were added. The reaction mixture was stirred at 0 °C for 15 min and at room temperature for 1 h. Ethanolamine (0.023 mL, 0.38 mmol) was added and the stirring was continued at room temperature for 1.5 h. H_2O (15 mL) was added to the purple reaction mixture and it was extracted with EtOAc (30 mL). The organic phase was washed with a 1 M aqueous solution of HCl (15 mL) and a saturated aqueous solution of $NaHCO_3$ (15 mL), dried over anhydrous Na_2SO_4, filtered and evaporated to provide a purple oil. The crude product was purified by flash chromatography (EtOAc/MeOH 1:0 → 19:1) to give **28** as a purple tar (0.045 g, 87%). ^1H NMR (400 MHz, $CDCl_3$) δ 9.57 (d, J = 10.4 Hz, 1H), 8.42 (d, J = 10.0 Hz, 1H), 8.14 (d, J = 4.0 Hz, 1H), 7.88 (dd, J = 10.4, 1.6 Hz, 1H), 7.82 (d, J = 10.0, 1.6 Hz, 1H), 7.42–7.35 (m, 3H), 7.27 (d, J = 4.0 Hz, 1H), 7.13–7.10 (m, 1H), 7.06 (t, J = 5.6 Hz, 1H), 3.91 (t, J = 5.0 Hz, 2H), 3.87 (s, 3H), 3.72–3.68 (m, 2H), 2.17 (s, 1H). ^{13}C NMR (101 MHz, $CDCl_3$) δ 192.8, 170.5, 159.7, 145.4, 144.7, 144.3, 142.2, 141.9, 138.0, 137.8, 129.3, 126.7, 125.9, 125.9, 122.4, 118.9, 117.9, 114.3, 62.1, 55.6, 43.5. HRMS (ESI-QTOF) *m/z*: $[M + H]^+$ Calcd for $C_{21}H_{20}NO_4$ 350.1392; Found 350.1391.

Methyl 1-benzoyl-1*H*-indole-5-carboxylate (31): Benzoyl chloride (0.12 mL, 1.0 mmol) and trimethylamine (0.14 mL, 1.0 mmol) were added to a solution of methyl indole-5-carboxylate (0.18 g. 1.0 mmol) in anhydrous DCM (1 mL) under argon. The resulting mixture was stirred at room temperature for 23 h. The reaction mixture was diluted with DCM (30 mL) and it was washed with a 1 M aqueous solution of HCl (15 mL), a saturated solution of $NaHCO_3$ (15 mL) and brine (15 mL), dried over anhydrous Na_2SO_4, filtered and evaporated to provide a brownish solid. The crude product was purified by flash chromatography (manual gradient of *n*-hexane/EtOAc 9:1 → 1:3) to give **31** as a white, amorphous solid (0.17 g, 59%). ^1H NMR (400 MHz, $CDCl_3$) δ 8.41 (d, J = 8.8 Hz, 1H), 8.34 (dd, J = 1.6, 0.8 Hz, 1H), 8.08 (dd, J = 8.8, 1.6 Hz, 1H), 7.77–7.74 (m, 2H), 7.65–7.61 (m, 1H), 7.56–7.52 (m, 2H), 7.38 (d, J = 3.6 Hz, 1H), 6.69 (dd, J = 4.0, 0.8 Hz, 1H), 3.96 (s, 3H). ^{13}C NMR (101 MHz, $CDCl_3$) δ 168.8, 167.5, 138.8, 134.2, 132.4, 130.7, 129.4, 128.9, 128.8, 126.3, 125.9, 123.3, 116.1, 108.9, 52.25. HRMS (ESI-QTOF) *m/z*: $[M + H]^+$ Calcd for $C_{17}H_{14}NO_3$ 280.0974; Found 280.0976.

Methyl 1-benzoyl-1*H*-indole-6-carboxylate (32): The same procedure as described above was repeated with methyl indole-6-carboxylate (0.18 g, 1.0 mmol) to give **32** as a white, amorphous solid (0.060 g, 22%). ^1H NMR (400 MHz, $CDCl_3$) δ 9.08 (m, 1H), 8.03 (dd, J = 8.2, 1.4 Hz, 1H), 7.77–7.74 (m, 2H), 7.66–7.61 (m, 2H), 7.57–7.53 (m, 2H), 7.46 (d, J = 4.0 Hz, 1H), 6.66 (d, J = 4.0, 0.8 Hz, 1H), 3.95 (s, 3H). ^{13}C NMR (101 MHz, $CDCl_3$) δ 168.6, 167.7, 135.6, 134.6, 134.2, 132.4, 130.6, 129.4, 128.9, 126.9, 125.3, 120.7, 118.3, 108.4, 52.27. HRMS (ESI-QTOF) *m/z*: $[M + H]^+$ Calcd for $C_{17}H_{14}NO_3$ 280.0974; Found 280.0974.

General procedure for the synthesis of compounds 33–36: Appropriate indole derivative was dissolved in anhydrous 1,4-dioxane (2.5 mL) under argon. *N,N*-Dimethylbenzamide (4.3 equiv for **33**, **35**, **36** or 1.0 equiv for **34**) and $POCl_3$ (4.3 equiv for **33**, **35**, **36** or 1.0 equiv for **34**) were added. The resulting solution was heated under microwave irradiation at 100 °C for 1–3 h. The red reaction mixture was poured into 1 M aqueous solution of NaOH (40 mL) on ice bath and extracted with DCM (25 + 15 mL). The organic phases were combined, washed with water (20 mL), dried over anhydrous Na_2SO_4, filtered, and evaporated to provide a crude product, which was purified by flash chromatography.

Methyl 3-benzoyl-1*H*-indole-5-carboxylate (33): Methyl indole-5-carboxylate (0.18 g, 1.0 mmol) with 1 h heating gave an orange oil, which after flash chromatography (manual gradient of *n*-hexane/EtOAc 9:1 → EtOAc) gave a yellow solid. The solid was washed a small amount of acetone to give **33** as a white, amorphous solid (0.009 g, 3%). ^1H NMR (400 MHz, DMSO-d_6) δ 12.39 (s, 1H), 8.96 (dd, J = 1.6, 0.8 Hz, 1H), 8.10 (s, 1H), 7.89 (dd, J = 8.6, 1.8 Hz, 1H), 7.84–7.81 (m, 2H), 7.66–7.61 (m, 2H), 7.58–7.54 (m, 2H), 3.89 (s, 3H). ^{13}C NMR (101 MHz, DMSO-d_6) δ 189.9, 167.0, 140.0, 139.4, 137.5, 131.4, 128.5, 128.5, 125.9, 124.1, 123.8, 123.3, 115.6, 112.4, 51.9. HRMS (ESI-QTOF) *m/z*: $[M + H]^+$ Calcd for $C_{17}H_{14}NO_3$ 280.0974; Found 280.0977.

Methyl 3-benzoyl-1*H*-indole-6-carboxylate (34): Methyl indole-6-carboxylate (0.18 g, 1.0 mmol) with 3 h heating gave an orange oil, which after flash chromatography (manual gradient of *n*-hexane/EtOAc 9:1 → EtOAc) gave a yellow solid. The solid was washed a small amount of acetone to give **34** as a white, amorphous solid (0.007 g, 2.5%). ^{1}H NMR (400 MHz, DMSO-d_6) δ 12.39 (s, 1H), 8.33 (dd, J = 8.4, 0.8 Hz, 1H), 8.18 (s, 1H), 8.16 (dd, J = 1.6, 0.8 Hz, 1H), 7.86 (dd, J = 8.4, 1.6 Hz, 1H), 7.82–7.80 (m, 2H), 7.65–7.61 (m, 1H), 7.58–7.54 (m, 2H), 3.89 (s, 3H). ^{13}C NMR (101 MHz, DMSO-d_6) δ 189.9, 166.7, 140.1, 138.6, 136.2, 131.3, 130.0, 128.5, 128.4, 124.2, 122.5, 121.3, 115.1, 114.0, 52.02. HRMS (ESI-QTOF) *m/z*: [M + H]$^+$ Calcd for $C_{17}H_{14}NO_3$ 280.0974; Found 280.0976.

Methyl 1,3-dibenzoyl-1*H*-indole-5-carboxylate (35): Methyl indole-5-carboxylate (0.18 g, 1.0 mmol) with 3 h heating gave an orange oil, which after flash chromatography (manual gradient of *n*-hexane/EtOAc 9:1 → EtOAc) gave **35** as a white, amorphous solid (0.090 g, 23%). ^{1}H NMR (400 MHz, $CDCl_3$) δ 9.02 (dd, J = 1.8, 0.6 Hz, 1H), 8.30 (dd, J = 8.8, 0.4 Hz, 1H), 8.17 (dd, J = 8.8, 0.8 Hz, 1H), 7.86–7.84 (m, 3H), 7.80–7.77 (m, 2H), 7.69–7.65 (m, 1H), 7.61–7.54 (m, 3H), 7.51–7.46 (m, 2H), 3.97 (s, 3H). ^{13}C NMR (101 MHz, $CDCl_3$) δ 190.7, 168.6, 167.2, 139.1, 139.1, 135.6, 133.4, 132.9, 132.6, 129.7, 129.2, 129.1, 128.8, 128.4, 127.6, 127.4, 124.8, 120.5, 115.8, 52.34. HRMS (ESI-QTOF) *m/z*: [M + H]$^+$ Calcd for $C_{24}H_{18}NO_4$ 384.1236; Found 384.1238.

Methyl 1,3-dibenzoyl-1*H*-indole-6-carboxylate (36): Methyl indole-6-carboxylate (0.18 g, 1.0 mmol) with 2 h heating gave an orange oil, which after flash chromatography (manual gradient of *n*-hexane/EtOAc 9:1 → EtOAc) gave **36** as a white, amorphous solid (0.19 g, 48%). ^{1}H NMR (400 MHz, $CDCl_3$) δ 8.97 (dd, J = 1.6, 0.8 Hz, 1H), 8.35 (dd, J = 4.4, 0.8 Hz, 1H), 8.15 (dd, J = 8.2, 1.4 Hz, 1H), 7.92 (s, 1H), 7.86–7.83 (m, 2H), 7.81–7.78 (m, 2H), 7.70–7.65 (m, 1H), 7.61–7.55 (m, 3H), 7.50–7.46 (m, 2H), 3.97 (s, 3H). ^{13}C NMR (101 MHz, $CDCl_3$) δ 190.8, 168.4, 167.2, 139.1, 136.9, 136.2, 133.4, 133.0, 132.7, 132.2, 129.7, 129.2, 129.1, 128.8, 128.1, 126.5, 122.4, 120.2, 117.8, 52.44. HRMS (ESI-QTOF) *m/z*: [M + H]$^+$ Calcd for $C_{24}H_{18}NO_4$ 384.1236; Found 384.1236.

General procedure for the synthesis of compounds 40–44: A 2 M solution of Me_2NH in THF (2.5 equiv) was added dropwise to a 0.67 M solution of appropriate acid chloride derivative (1 equiv) in anhydrous DCM (1.5 mL/mmol) on ice bath under argon. The resulting mixture was stirred at 0 °C for 45–150 min. The reaction mixture was quenched by a 1 M aqueous solution of HCl (25 mL) on ice bath and DCM (30 mL) was added. The organic phase washed with a 1 M aqueous solution of HCl (25 mL), a saturated aqueous solution of $NaHCO_3$ (25 mL) and brine (25 mL), dried over anhydrous Na_2SO_4, filtered and evaporated to give a crude product which was used in the next step without further purification.

4-Methoxy-*N*,*N*-dimethylbenzamide (40): 4-Methoxybenzoyl chloride (0.68 g, 4.0 mmol) gave **40** as a yellowish oil (0.55, 76%). ^{1}H NMR (400 MHz, $CDCl_3$) δ 7.41–7.38 (m, 2H), 6.91–6.88 (m, 2H), 3.82 (s, 3H), 3.05 (s, 6H). ^{13}C NMR (101 MHz, $CDCl_3$) δ 171.6, 160.7, 129.3, 128.6, 113.7, 55.46. HRMS (ESI-QTOF) *m/z*: [M + H]$^+$ Calcd for $C_{10}H_{14}NO_2$ 180.1024; Found 180.1023.

3-Methoxy-*N*,*N*-dimethylbenzamide (41): 3-Methoxybenzoyl chloride (0.56 mL, 4.0 mmol) gave **41** as a yellow oil (0.69 g, 96%). ^{1}H NMR (400 MHz, $CDCl_3$) δ 7.32–7.27 (m, 1H), 6.97–6.91 (m, 3H), 3.81 (s, 3H), 3.08 (s, 3H), 2.98 (s, 3H). ^{13}C NMR (101 MHz, $CDCl_3$) δ 171.5, 159.7, 137.8, 129.6, 119.3, 115.5, 112.5, 55.5, 39.6, 35.4. HRMS (ESI-QTOF) *m/z*: [M + H]$^+$ Calcd for $C_{10}H_{14}NO_2$ 180.1025; Found 180.1025.

Methyl 3-(dimethylcarbamoyl)benzoate (42): Methyl 3-(chlorocarbonyl)benzoate (0.79 g, 4.0 mmol) gave **42** as a yellow oil (0.82 g, 99%). ^{1}H NMR (400 MHz, $CDCl_3$) δ 8.07–8.03 (m, 2H), 7.61–7.58 (m, 1H), 7.49–7.44 (m, 1H), 3.90–3.89 (m, 3H), 3.09 (s, 3H), 2.95 (s, 3H). ^{13}C NMR (101 MHz, $CDCl_3$) δ 170.6, 166.4, 136.7, 131.6, 130.6, 130.4, 128.7, 128.2, 52.4, 39.6, 35.5. HRMS (ESI-QTOF) *m/z*: [M + H]$^+$ Calcd for $C_{11}H_{14}NO_3$ 208.0970; Found 208.0970.

***N*,*N*-Dimethyl-2-phenylacetamide (43):** Phenylacetyl chloride (0.53 mL, 4.0 mmol) gave **43** as a yellowish solid (0.63 g, 97%). ^{1}H NMR (400 MHz, $CDCl_3$) δ 7.34–7.30 (m, 2H), 7.27–7.22 (m, 3H), 3.72 (s, 2H), 3.00 (s, 3H), 2.97 (s, 3H). ^{13}C NMR (101 MHz, $CDCl_3$) δ 171.1, 135.2, 128.9, 128.8, 126.8, 41.2, 37.8, 35.7. HRMS (ESI-QTOF) *m/z*: [M + H]$^+$ Calcd for $C_{10}H_{14}NO$ 164.1075; Found 164.1074.

***N*,*N*-Dimethylthiophene-2-carboxamide (44):** 2-Thiophenecarbonyl chloride (0.43 mL, 4.0 mmol) gave **44** as a yellow oil (0.60 g, 96%). ^{1}H NMR (400 MHz, $CDCl_3$) δ 7.44 (dd, J = 5.0, 1.0 Hz, 1H), 7.35 (dd, J = 3.6, 1.2 Hz, 1H), 7.04 (dd, J = 4.8, 3.6 Hz, 1H), 3.18 (s, 6H). ^{13}C NMR (101 MHz, $CDCl_3$) δ 164.6, 138.1, 129.3, 128.9, 126.8. HRMS (ESI-QTOF) *m/z*: [M + H]$^+$ Calcd for $C_7H_{10}NOS$ 156.0483; Found 156.0484.

Biology

Materials: Human orexin-A was from NeoMPS (Strasbourg, France), probenecid was from Sigma-Aldrich (St. Luis, MO), and SB-334867, i.e. *N*-biphenyl-2-yl-1-[[(1-methyl-1*H*-benzimidazol-2-yl)sulfanyl]acetyl]-L-prolinamide and TCS-1102, i.e. *N*-(2-methyl-6-benzoxazolyl)-*N*′-1,5-naphthyridin-4-yl urea from Tocris Bioscience (Bristol, UK).

Cell culture and Media: CHO-hOX_1 and -hOX_2 cells,[27,37] and control CHO-K1 cells (not expressing orexin receptors; control CHO cells), were cultured in Ham's F12 medium (Gibco/Life Technologies, Paisley, UK) + supplements on plastic cell culture dishes (56 cm^2 bottom area; Greiner Bio-One GmbH, Frickenhausen, Germany) as described in reference[29]. We used black clear-bottom half-area Cellstar µClear 96-well cell culture plates (Greiner Bio-One GmbH; Frickenhausen, Germany) with polyethyleneimine (25 µg/mL for 1 h at 37 °C; Sigma-Aldrich, St. Louis, MO, USA) coating. Hepes-buffered medium (HBM; 137 mM NaCl, 5 mM KCl, 1.2 mM $MgCl_2$, 0.44 mM KH_2PO_4, 4.2 mM $NaHCO_3$, 1 mM $CaCl_2$, 10 mM glucose, 20 mM HEPES and 0.1% (w/v) stripped bovine serum albumin, and adjusted to pH 7.4 with NaOH) was used as the experimental medium.

Ca^{2+} elevation: Measurements were conducted essentially as described before.[25,26] The cells, 1.5×10^4 per well, were plated, and twenty-four hours later, cell culture medium removed and the cells loaded with the loading solution composed of FLIPR Calcium 4 Assay Kit (Molecular Devices, Sunnyvale, CA, USA) dissolved in and diluted with HBM + 1 mM probenecid, for 60 min at 37 °C. Then, the plate was measured in a FlexStation 3 fluorescence plate reader (Molecular Devices); the intracellular Ca^{2+} levels were read as fluorescence changes (excitation at 485 nm, emission at 525 nm) at 37 °C, for 150 s with 30 s of baseline for each well. For agonist studies, antagonists SB-334867 (10 µM, on OX_1) and TCS-1102 (10 µM, on OX_2) were added to the wells manually, when applicable, and incubated for 30 min before the measurement, after which the test compounds were added by FlexStation, and the plate was measured as described above. For potentiation studies the orexin-A/compound and ATP/compound mixtures were added by FlexStation as a single addition, and then measured as the agonist plates. For the agonist and potentiation screens, the measurements were conducted in triplicate three individual times. The concentration-response data were measured in triplicate 3–6 individual times.

In the agonist activity studies, vehicle (buffer) addition served as a negative control for the test compound concentrations up to 10 µM. With the test compound concentrations 18 µM, 32 µM and 45 µM, the DMSO concentration was 0.18–0.45% accordingly; to rule out the effects of DMSO on the observed responses, the corresponding DMSO additions were used as negative controls. Additionally, 100 nM orexin-A and 100 µM ATP were used as positive controls in the orexin receptor-expressing cells, and 100 µM ATP in the control CHO cells. When assessing the potentiation of the response to orexin-A, 10 nM and 30 nM ATP was used as negative controls as described in reference[12], while 100 nM orexin-A served as a positive control. In case of potentiating the effects of ATP, vehicle (buffer) served as a negative control and 100 µM ATP as a positive control.

Data analysis: All data are presented as mean ± SEM. Microsoft Excel was used for data visualizations and analyses as described in reference[20]. Student's paired two-tailed t-test was used for the statistical comparisons. Significances are as follows: $P > 0.05$; $*P < 0.05$; $**P < 0.01$; $***P < 0.001$.

All responses were separately normalized to the control orexin-A or ATP responses for each independent experiment before averaging (at concentrations corresponding E_{max} of orexin-A or ATP in the agonist measurements or EC_{20} in the potentiation measurements). Furthermore, in the analysis of the potentiation effect of compounds inducing Ca^{2+} elevation of their own, the full compound-induced Ca^{2+} elevation was subtracted from the responses to the orexin-A/compound and ATP/compound mixtures prior to the analysis.

Computational studies

Setup and analysis of the molecular dynamics simulations: The simulations have been described in reference[33]. Briefly, we utilized OX_2 crystal structure for the starting coordinates of the receptor for MD simulations (pdb ID: 4S0V[32]), and used Modeller 9.14[38] with default settings to fill the gaps in the crystal structure (residues 50–254 and 294–381) with 4S0V as a template. Protonation states were assigned automatically with Gromacs,[39] except for the $Asp100^{2.50}$, which was protonated. Compound **41** was docked to the crystal structure as described previously;[25] in short, we used Glide Induced Fit protocol with the crystallized binding site water molecules. Similarities to **43** (suvorexant) binding directed the pose selection. The binding pose was then copied into the homology model.

We generated a hexagonal membrane with 150 POPC lipids per leaflet and a second membrane with 126 POPC + 42 cholesterol per leaflet with Charmm-GUI,[40] and solvated the membranes in TIP3p water[41] to reach a height of 12 nm. Cholesterol locations next to the receptor were defined by a coarse-grained simulation. The receptor complex (with surrounding lipids in the case of the cholesterol membrane) was embedded into the membrane with the Gromacs'[39] tool *membed*. We neutralized the systems with NaCl and added it to 100 mmol/l concentration.

As a forcefield, we used Amber99sb-ildn[42] together with Slipids.[43] Compound **41** parameters were combined from Antechamber,[44] Amber99sb-ildn and OPSL-AA.[45] Simulations were run under periodic boundary conditions with a time step of 2 fs, temperature of 310 K (Nose–Hoover thermostat), and pressure of 1 bar (semi-isotropic Parrinnello–Rahman barostat for z- and xy-dimension). Cut-off of 1 nm was used for short-range electrostatics and vdW with long range dispersion corrections for energy and pressure and PME for electrostatics.

Each simulation was equilibrated for 70 ns; first 10 ns with 1000 kJ/mol restraints on protein and ligand heavy atoms. During the next 4 x 10 ns, the restraints were tapered off to 200 kJ/mol. Then the protein restrains were applied only to Cα for 10 ns, and for the final 10 ns, only to the Cα in the transmembrane helices. The ligand constraints remained unchanged in the last two steps. In case of cholesterol simulations, the close cholesterol was restrained (1000 kJ/mol) only in the first 10 ns phase. We simulated both systems for 3 µs with additional 1 µs replicas.

All simulations were concatenated and aligned on the receptor Cα. For frames every 0.3 ns, we used VMD's[46] tool *Volmap* in default settings to map the densities of different groups of compound **41** atoms.

QM calculations: The three dimensional structures and protonation states of the compounds **1**, **2**, **26**, **28**, **35**, **37**, **39** and **40** were prepared by LigPrep of Schrödinger Maestro 2016v3,[47] after which they were superimposed (flexible compound alignment by Maestro software), and energy-minimized. The Jaguar software[48] was used for the quantum mechanical calculations utilizing LMP2 theory with 6-31G** basis set (including a diffusion function) with default parameters. The presented dipole moments were calculated from the coupled perturbed Hartree-Fock (CPHF) wave function. Compound **37** possesses a negative charge and thus the calculation did not find positive ESP values for this compound; the ESP surfaces were thus visualised using two isovalues: -82 (compound **37**) and -47 (other compounds). As a control we calculated the electrostatic surface potential of non-substituted azulene scaffold—the obtained electron densities were in accordance with the literature (electron density of the azulene scaffold was located on the 5-membered ring; Supporting information Figure 3; see also references[49,50]). The numerical values of the experimental and calculated dipole moments were also of a similar magnitude, 1.08 ± 0.02 D[49], 1.0 ± 0.05[50], and 0.93 D (calculated).

Docking simulations: Compound **37** was docked to the crystal structure of OX_2 receptor (pdb ID: 5WQC[31]) using the Induced Fit protocol of Glide software,[51] and the binding site was defined by the location of the co-crystallized **42** (EMPA). Two of the co-crystallized water molecules of the **42** binding site were kept in the simulation (residue numbers 4022 and 4053). The utilized protocol was capable of reproducing the binding mode of **42** observed in the crystal structure.

Acknowledgements

Marja Peltola, Jouni Oksanen and Maiju K. Rinne are acknowledged for assistance with the experiments. Nina Sipari is acknowledged for the mass spectroscopy. CSC – IT Center for Science and the Hilife/Biocenter Finland Drug Discovery and Chemical Biology (DDCB) network are acknowledged for organizing computational resources in the H.X. group. T.O.L. thanks the Magnus Ehrnrooth Foundation, Oskar Öflunds Stiftelse sr, the Finnish Pharmaceutical Society and the Doctoral Program in Drug Research of the University of Helsinki, A.T. thanks the Finnish Cultural Foundation and the Orion Research Foundation, and J.P.K the Magnus Ehrnrooth Foundation and the Liv & Hälsa Foundation for financial support.

Keywords: 1-benzoylazulene • Orexin receptor • Biological activity • Drug discovery • Medicinal chemistry

References:

[1] T. Sakurai, A. Amemiya, M. Ishii, I. Matsuzaki, R. M. Chemelli, H. Tanaka, S. C. Williams, J. A. Richardson, G. P. Kozlowski, S. Wilson, et al., *Cell* **1998**, *92*, 573–585.

[2] L. de Lecea, T. S. Kilduff, C. Peyron, X.-B. Gao, P. E. Foye, P. E. Danielsson, C. Fukuhara, E. L. F. Battenberg, V. T. Gautvik, F. S. Bartlett II, et al., *Proc. Natl. Acad. Sci.* **1998**, *95*, 322–327.

[3] A. L. Gotter, A. J. Roecker, R. Hargreaves, P. J. Coleman, C. J. Winrow, J. J. Renger, *Prog. Brain Res.* **2012**, *198*, 163–196.

[4] S. Bingham, P. T. Davey, A. J. Babbs, E. A. Irving, M. J. Sammons, M. Wyles, P. Jeffrey, L. Cutler, I. Riba, A. Johns, et al., *Pain* **2001**, *92*, 81–90.

[5] G. James, M.H., Mahler, S. V., Moorman, D.E., Aston-Jones, *A Decade of Orexin/Hypocretin and Addiction: Where Are We Now?*, Springer, Cham., **2017**.

[6] M. H. James, E. J. Campbell, C. V. Dayas, in *Behav. Neurosci. Orexin/Hypocretin. Curr. Top. Behav. Neurosci.* (Eds.: A. Lawrence, L. de Lecea), Springer, Cham, **2017**.

[7] A. J. Roecker, C. D. Cox, P. J. Coleman, *J. Med. Chem.* **2016**, *59*, 504–530.

[8] T. Nagahara, T. Saitoh, N. Kutsumura, Y. Irukayama-Tomobe, Y.

Ogawa, D. Kuroda, H. Gouda, H. Kumagai, H. Fujii, M. Yanagisawa, et al., *J. Med. Chem.* **2015**, *58*, 7931–7937.

[9] M. K. Rinne, T. O. Leino, A. Turku, P. M. Turunen, Y. Steynen, H. Xhaard, E. A. A. Wallén, J. P. Kukkonen, *Eur. J. Pharmacol.* **2018**, *837*, 137–144.

[10] Y. Irukayama-Tomobe, Y. Ogawa, H. Tominaga, Y. Ishikawa, N. Hosokawa, S. Ambai, Y. Kawabe, S. Uchida, R. Nakajima, T. Saitoh, et al., *Proc. Natl. Acad. Sci.* **2017**, *114*, 5731–5736.

[11] T. Voisin, A. El Firar, M. Fasseu, C. Rouyer-Fessard, V. Descatoire, F. Walker, V. Paradis, P. Bedossa, D. Henin, T. Lehy, et al., *Cancer Res.* **2011**, *71*, 3341–3351.

[12] T. O. Leino, A. Turku, J. Yli-Kauhaluoma, J. P. Kukkonen, H. Xhaard, E. A. A. Wallén, *Eur. J. Med. Chem.* **2018**, *157*, 88–100.

[13] S. Löber, N. Tschammer, H. Hübner, M. R. Melis, A. Argiolas, P. Gmeiner, *ChemMedChem* **2009**, *4*, 325–328.

[14] L. Karhu, A. Turku, H. Xhaard, *BMC Struct. Biol.* **2015**, *15*, 1–17.

[15] K. Yanagisawa, Takashi; Wakabayashi, Shuichi; Tomiyama, Tsuyoshi; Yasunami, Masafumi; Takase, *Chem. Pharm. Bull.* **1988**, *36*, 641–647.

[16] K. Ikegai, M. Imamura, T. Suzuki, K. Nakanishi, T. Murakami, E. Kurosaki, A. Noda, Y. Kobayashi, M. Yokota, T. Koide, et al., *Bioorg. Med. Chem.* **2013**, *21*, 3934–3948.

[17] C. Chen, O. Lee, C. Yao, M. Chuang, Y. Chang, M. Chang, Y. Wen, W. Yang, C. Ko, N. Chou, et al., *Bioorg. Med. Chem. Lett.* **2010**, *20*, 6129–6132.

[18] S. Löber, H. Hübner, A. Buschauer, F. Sanna, A. Argiolas, M. R. Melis, P. Gmeiner, *Bioorg. Med. Chem. Lett.* **2012**, *22*, 7151–7154.

[19] M. S. M. Timmer, B. L. Stocker, P. T. Northcote, B. A. Burkett, *Tetrahedron Lett.* **2009**, *50*, 7199–7204.

[20] J. P. Kukkonen, *Cell. Signal.* **2016**, *28*, 51–60.

[21] J. Putula, T. Pihlajamaa, J. P. Kukkonen, *Br. J. Pharmacol.* **2014**, *171*, 5816–5828.

[22] J. Putula, P. M. Turunen, L. Johansson, J. Näsman, R. Ra, L. Korhonen, J. P. Kukkonen, *FEBS Lett.* **2011**, *585*, 1368–1374.

[23] D. Smart, C. Sabido-David, S. J. Brough, F. Jewitt, A. Johns, R. A. Porter, J. C. Jerman, *Br. J. Pharmacol.* **2001**, *132*, 1179–1182.

[24] J. M. Bergman, A. J. Roecker, S. P. Mercer, R. a. Bednar, D. R. Reiss, R. W. Ransom, C. Meacham Harrell, D. J. Pettibone, W. Lemaire, K. L. Murphy, et al., *Bioorganic Med. Chem. Lett.* **2008**, *18*, 1425–1430.

[25] A. Turku, A. Borrel, T. O. Leino, L. Karhu, J. P. Kukkonen, H. Xhaard, *J. Med. Chem.* **2016**, *59*, 8263–8275.

[26] A. Turku, M. K. Rinne, G. Boije af Gennäs, H. Xhaard, D. Lindholm, J. P. Kukkonen, *PLoS One* **2017**, *12*, e0178526.

[27] P.-E. Lund, R. Shariatmadari, A. Uustare, M. Detheux, M. Parmentier, J. P. Kukkonen, K. E. O. Åkerman, *J. Biol. Chem.* **2000**, *275*, 30806–30812.

[28] S. Ammoun, L. Johansson, M. E. Ekholm, T. Holmqvist, A. S. Danis, L. Korhonen, O. A. Sergeeva, H. L. Haas, K. E. O. Åkerman, J. P. Kukkonen, *Mol. Endocrinol.* **2006**, *20*, 80–99.

[29] M. H. Jäntti, J. Putula, P. Somerharju, M. Frohman, J. P. Kukkonen, *Br. J. Pharmacol.* **2012**, *165*, 1109–23.

[30] P. M. Turunen, M. H. Jantti, J. P. Kukkonen, *Mol Pharmacol* **2012**, *82*, 156–167.

[31] R. Suno, K. T. Kimura, T. Nakane, K. Yamashita, J. Wang, T. Fujiwara, Y. Yamanaka, D. Im, S. Horita, H. Tsujimoto, et al., *Structure* **2018**, *26*, 7–19.e5.

[32] J. Yin, J. C. Mobarec, P. Kolb, D. M. Rosenbaum, *Nature* **2015**, *519*, 247–250.

[33] L. V Karhu, A. Magarkar, A. Bunker, H. G. Xhaard, *J. Phys. Chem. B* **2019**, DOI 10.1021/acs.jpcb.8b10220.

[34] C. J. Winrow, A. L. Gotter, C. D. Cox, S. M. Doran, P. L. Tannenbaum, M. J. Breslin, S. L. Garson, S. V Fox, C. M. Harrell, J. Stevens, et al., *J. Neurogenet.* **2011**, *25*, 52–61.

[35] P. Malherbe, E. Borroni, L. Gobbi, H. Knust, M. Nettekoven, E. Pinard, O. Roche, M. Rogers-Evans, J. G. Wettstein, J. L. Moreau, *Br. J. Pharmacol.* **2009**, *156*, 1326–1341.

[36] R. Mould, J. Brown, F. H. Marshall, C. J. Langmead, *Br. J. Pharmacol.* **2014**, *171*, 351–363.

[37] S. Ammoun, T. Holmqvist, R. Shariatmadari, H. B. Oonk, M. Detheux, M. Parmentier, *J Pharmacol Exp Ther* **2003**, *305*, DOI 10.1124/jpet.102.048025.

[38] A. Säli, T. L. Blundell, *J Mol Biol* **1993**, *234*, DOI 10.1006/jmbi.1993.1626.

[39] M. J. Abraham, T. Murtola, R. Schulz, S. Páll, J. C. Smith, B. Hess, E. Lindahl, *SoftwareX* **2015**, *1–2*, 19–25.

[40] S. Jo, T. Kim, V. G. Iyer, W. Im, *J. Comput. Chem.* **2008**, *29*, 1859–1865.

[41] W. L. Jorgensen, J. Chandrasekhar, J. D. Madura, R. W. Impey, M. L. Klein, *J. Chem. Phys.* **1983**, *79*, 926–935.

[42] K. Lindorff-Larsen, S. Piana, K. Palmo, P. Maragakis, J. L. Klepeis, R. O. Dror, D. E. Shaw, *Proteins* **2010**, *78*, 1950–1958.

[43] J. P. M. Jämbeck, A. P. Lyubartsev, *J. Chem. Theory Comput.* **2013**, *9*, 774–784.

[44] D. A. Case, V. Babin, J. T. Berryman, R. M. Betz, Q. Cai, D. S. Cerutti, T. E. Cheatham, T. A. Darden, R. E. Duke, H. Gohlke, et al., **2014**.

[45] G. A. Kaminski, R. A. Friesner, J. Tirado-Rives, W. L. Jorgensen, *J. Phys. Chem. B* **2001**, *105*, 6474–6487.

[46] W. Humphrey, A. Dalke, K. Schulten, *J. Mol. Graph.* **1996**, *14*, 33–38.

[47] Schrödinger. Small-Molecule Drug Discovery Suite 2016-3: LigPrep; Schrödinger, LLC: New York, NY, **2016**.

[48] A. D. Bochevarov, E. Harder, T. F. Hughes, J. R. Greenwood, D. A. Braden, D. M. Philipp, D. Rinaldo, M. D. Halls, J. Zhang, R. A. Friesner, *Int. J. Quantum Chem.* **2013**, *113*, 2110–2142.

[49] A. G. Anderson, B. M. Steckler, *J. Am. Chem. Soc.* **1959**, *81*, 4941–4946.

[50] G. W. Wheland, D. E. Mann, *J. Chem. Phys.* **1949**, *17*, 264–268.

[51] Schrödinger. Small-Molecule Drug Discovery Suite 2016-3: Schrödinger Suite 2016-3 Induced Fit Docking Protocol; Glide Version 7.2; Prime Version 4.5; Schrödinger, LLC: New York, NY, **2016**.

10.1002/cmdc.201900074

Entry for the Table of Contents

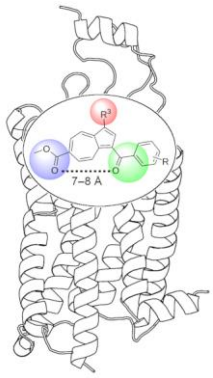

Synthesis and biological evaluation of novel 1-benzoylazulene and 1- and 3-benzoylindole derivatives lead to identification of weak OX_1 and OX_2 orexin receptor agonists and compounds potentiating the effects of orexin-A. SAR and computational studies highlighted the presence of two hydrogen bond acceptors within 7–8 Å of each other in the orexin receptor activators, but not antagonists nor inactive compounds.